6-2021

Flow Visualization of Bolus Microcapsule Delivery through 3D Printed Microneedles

Sophie Quisling

Leana Vestal

Alexis Enstrom

SANTA CLARA UNIVERSITY

Department of Bioengineering

I HEREBY RECOMMEND THAT THE THESIS PREPARED
UNDER MY SUPERVISION BY

Sophie Quisling, Leana Vestal, and Alexis Enstrom

ENTITLED

Flow Visualization of Bolus Microcapsule Delivery through 3D Printed Microneedles

BE ACCEPTED IN PARTIAL FULFILLMENT OF THE REQUIREMENTS
FOR THE DEGREE OF

BACHELOR OF SCIENCE
IN
BIOENGINEERING

M. Mobed-Miremadi 6/10/2021

Thesis Advisor(s) (Maryam Mobed-Miremadi) date

6/10/2021

Department Chair(s) (use separate line for each chair) date

Flow Visualization of Bolus Microcapsule Delivery through 3D Printed Microneedles

By

Sophie Quisling, Leana Vestal, and Alexis Enstrom

SENIOR DESIGN PROJECT REPORT

Submitted to

the Department of BioEngineering

of

SANTA CLARA UNIVERSITY

in Partial Fulfillment of the Requirements

for the degree of

Bachelor of Science in BioEngineering

Santa Clara, California

2021

Abstract

Microneedle arrays are an emerging technology that offers a novel drug delivery system to treat a variety of skin wounds and diseases. The needles deliver therapeutics to the epidermis layer of the skin and therefore establish advantageous qualities over the standard hypodermic needle as they are non-invasive, efficient in biologic absorption, and can be self-administered. This project investigates a custom 3D-printed hollow microneedle device created by a Santa Clara University Senior Design team in 2018 for microencapsulated cell extrusion to be applied for accelerated wound healing. The goal of our project is to operate in the therapeutic range for flowrate and pressure to minimize patient pain and improve patient compliance. Simulations of laminar flow and particle tracing through the 3D-printed microneedle device pre-puncture were generated using COMSOL Multiphysics software. These results established a robust flow profile for fluid flow and encapsulated cell tracing through the device when operating in optimal conditions. Next various failure modes were analyzed to determine their effects on the flow profile. Tip deformation, nozzle clogging, and suction were modelled using COMSOL, and respective provisions were added to a failure modes and effects analysis (FMEA) matrix. In future experiments, the generated flow patterns may be used as a machine learning data training set to implement an algorithm that recognizes and predicts failure modes based on flow profiles. Additionally, in situ flow data will be collected to compose a more robust model.

Keywords: hollow microneedle, 3D printing, laminar flow, particle trajectory, encapsulated cells.

Acknowledgements

Our group would like to offer thanks to those who contributed and supported our senior design project: The School of Engineering and the Bioengineering Department for the resources that allowed us to have the software required for our progress.

And finally, a special thank you to our advisor Dr. Mobed-Miremadi who guided us through our project despite being in a global pandemic. She kept us motivated and demonstrated inspiring commitment to the success of our project.

TABLE OF CONTENTS

LIST OF FIGURES:

Figure 19. (a) Reynold's number plotted as a function of height in millimeters through the center of the device. (b) The stagnation zone detected in Plot A at height 4.73 mm.

Figure 20. Velocity profiles across horizontal cutlines at locations V1-V4 as specified in Figure 8.

Figure 21. Velocity, pressure, and particle trajectory plots demonstrating suction on the center needle with an increased diameter of 600 microns.

Figure 22. (a) One dimensional graph of impact force plot of 5 needles with center nozzle at a 600 micrometres in diameter. (b) Plane plot of impact force of all 15 needles with center nozzle at a 600 micrometer diameter.

Figure 23. 2D velocity, pressure, and particle trajectory plots demonstrating a slanted center nozzle

LIST OF TABLES:

Chapter 1 - Microneedle Arrays and Transdermal Drug Delivery

1.1 Introduction

The introduction chapter will provide the background information relevant to understanding our design project and an overview of our project's objectives. Microneedle technology, encapsulation of cells, and the VAS scale for pain metric formulation will establish the background knowledge necessary to comprehend the importance of our design project.

1.1.1 Problem Statement

Microneedles offer painless therapeutic delivery and withdrawal of biological components through the dermis layer of the skin. Our project addresses the demand of non-invasive medical devices for drug delivery to minimize patient pain and induce improved patient compliance. By operating within this therapeutic range, we will simulate laminar flow and microcapsule trajectory through our 3D printed microneedle device in the pre-puncture stage. Using the validated model, we will examine several failure modes in which the microneedles could undergo due to 3D printing and determine their effect on flow profiles.

1.1.2 Project Proposal

Our project will be a continuation of previous years, which worked to capture the benefits of cell-hydrogel therapies delivered by 3D printed micro-needles. This system is minimally invasive, optimally painless, and offers treatment directly to the affected area. Our goal is to minimize patient pain by optimizing the flow rate of suspended cells through the microneedles. We also aim to test the reliability of continuous extrusion through all thirteen microneedles to verify the treatment’s effectiveness.

Our project will contain two main goals for the 3D printed microneedles. For our first goal, we will be to model laminar flow and particle trajectory in fluid flow through the microneedles using COMSOL. We will model flow through a single needle in 2D and in 3D, as well as the flow through the entire device in 2D and 3D. If allowed access into the lab, we would be verifying the pressure of the flow for pain minimization using pressure sensitive tape. Once we have validated our device using therapeutic ranges for flow rate and microcapsule extrusion, we will model several failure modes that our device has the potential to undergo due to 3D printing errors, microencapsulated cell errors, and human errors. To investigate the pain levels experienced by patients, the pressure will be analyzed using pressure sensitive film if allowed into the lab. Pressure sensitive film will simulate skin, where color change intensity indicates the pressure experienced. This method will require some image analysis in order to collect data on the quantity of pressure the pressure tape experiences.

The target customers of the 3D printed microneedles are medical professionals in need of a non-invasive technique for drug delivery systems for therapeutics. The use of 3D printed microneedles is important as it is minimally invasive and reduces pain and anxiety in patients undergoing treatment.

1.1.3 Project Justification

The previous group that worked on this project determined microencapsulated cells can successfully be extruded from the microneedle device while maintaining viability. However, in the absence of laboratory access and the ability to quantify shear, the most logical step is flow visualization and in silico creation of failure modes. When conducted under therapeutic flow rates, flow visualization and particle tracing will generate predictive profiles of biologic delivery pre-puncture.

1.1.4 Medical Importance

Drug delivery methods that provide innovative techniques of administration are important in the medical field as individualized medicine is becoming a focus for treating patients with unique diseases. Transdermal drug delivery is a pressing field for drug delivery systems as this method is noninvasive and can be self-administered by patients. It is estimated that 20% of the adult population suffers from needle phobia and are more likely to avoid receiving the medical care they need [13]. By proposing a method of drug delivery that can minimize pain and be self-administered, patients will have an increased compliance to receiving medical attention. This is applicable in today's world as SARS-CoV-2 has been infecting and spreading to millions of people and a vaccine delivered by a hypodermic needle is currently the best method to help prevent spread of infection. The use of microneedles to deliver vaccines to people will potentially increase the amount of people willing to receive a vaccine. Once this technology is further developed, an entirely new, non-invasive, and reliable way of delivering cells to patients with various diseases will be available to patients.

1.1.5 Virtual Plan

Due to COVID-19 restrictions, we were not able to go into the lab to print and test our 3D microneedles and microencapsulated cell extrusion. Instead, we focused on validating the design of the 3D printed microneedles using COMSOL Multiphysics software. COMSOL is a cross-platform finite element analysis, solver, and multiphysics simulation. We utilized the software to test our design using different physics simulations including laminar flow and particle tracing in fluid flow. We also tested multiple failure modes of the 3D printed artifacts to determine their effects on flow profiles. Using COMSOL allowed us to keep our project virtual so we could all stay safe and help stop the spread of COVID-19.

1.1.6 Project Objectives

Our aims for the project are the following:

1. Model one phase flow with particle tracing to simulate microcapsule trajectory through a custom 3D printed device pre-puncture.
2. Validate model using COMSOL Multiphysics software to simulate multiple failure modes of 3D printed artifacts.

1.2 Background

1.2.1 Microneedle technology

The expansion of the microelectronics industry began in the 1990s, with the first success in developing a microneedle for the purpose of transdermal drug administration occurring in 1998 [5]. Transdermal drug delivery has various conditions it can be applied to, such as administering medicine to combat tumors, diabetes, wound treatment, and scar repair. There are many types of microneedles such as solid, coated, dissolving, hollow and porous microneedles. Transdermal drug delivery is commonly achieved by utilizing one type of microneedle array called hollow microneedle arrays which have been tested and developed for market production. Transdermal drug delivery is advantageous over injection-mediated and oral administration due to increased bioavailability, the fraction of the drug that enters the bloodstream and can contribute towards healing. Furthermore, its ability to be self-administered presents a large improvement as it increases the ease and accessibility of long-term drug administration over injection-mediated drugs. One disadvantage is the impermeability of the skin, however with the correct geometry and extrusion rates this can be overcome.

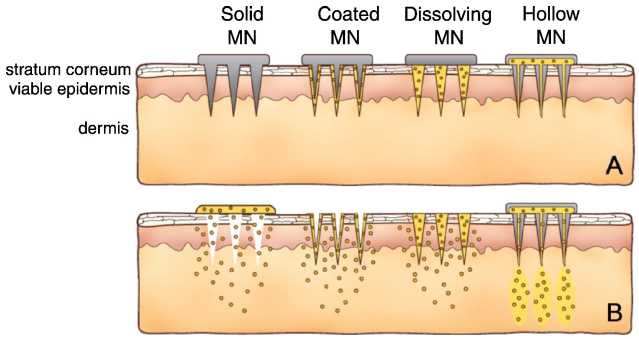

Figure 1. Various types of microneedles and how drugs are administered. [11]

The number of hollow microneedle publications increased drastically between 2008 and 2011 [2], during this time fabrication methods were being tested. Hollow microneedles are connected to a reservoir which contains drugs that must be delivered to the patient. The reservoir is advantageous because it allows larger quantities of drugs to be administered to the patient. However, the disadvantages of this method include the complexity of fabrication processes and specific application parameters which make it difficult to spread the use of this device

throughout drug delivery in various medical treatments. This type of microneedle utilizes diffusion or pressure-driven flow to dispense the drugs. The use of microneedles in drug delivery is favorable to traditional methods of drug delivery such as syringe needles or oral drug delivery due to:

- Ability to minimize pain through optimizing flow rates
- Ability to minimize pain through the dimensions of microneedles
- The direct absorption of drugs into blood circulation

1.2.2 Microencapsulation of particles

Microencapsulation was first patented in 1955 [16], this process protects cellular particles from the external environment without affecting the medicinal properties of the cells. Microencapsulation is most commonly used in pharmaceutical companies, as pills utilize this technology, encapsulating particles that will interact with the body's immune system once the capsule deteriorates. This method of drug administration is effective as it allows particles to be slowly released into the body.

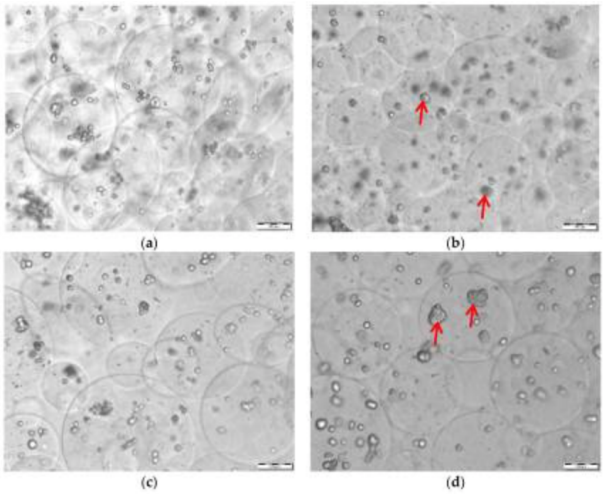

Figure 2. Encapsulation of HepG2 cells within alginate microcapsules. (a) 3.5% (w/v) alginate capsules 2 h post-fabrication (Set 1, control); (b) 3.5% (w/v) alginate capsules at 24 h post-fabrication (Set 2, control); (c) 3.5% (w/v) alginate extruded capsules 2 h post-fabrication (Set 1); and, (d) 3.5% (w/v) alginate capsules extruded 24 h post-fabrication (Set 2). Scale bar indicates 100μm.Red arrows represent spheroid formation.[5]

Figure 2 demonstrates the encapsulation of HepG2 cells extruded through a microneedle device performed by a Santa Clara Bioengineering team in 2018 [5]. Microencapsulated cell extrusion using 3D printed microneedles is a new area of application for microneedles. "Microencapsulation is a process by which individual particles of an active agent can be stored within a shell, surrounded or coated with a continuous film of polymeric material to produce particles in the micrometer to millimeter range, for protection and/or later release," [8]. Microencapsulation effectively delivers active compounds to treat deficiencies or combat the overgrowth of certain cells. It is imperative that microencapsulation:

- Protects the encapsulated compound
- Increases the stability and length of the viability of the product
- Controls the release of the compound.

Microencapsulation prohibits cell extrusion at first and then allows cells to be dispersed throughout the body. Cell extrusion is used in controlling cell counts and maintaining the function of the barrier. Combining the microencapsulation of cells with microneedles presents challenges as microneedles have been developed to deliver many types of drugs but not through microencapsulation. The design of the microneedle must be reconsidered for this technology as the shape and the speed of flow must limit the amount of shear stress on the extruded cells. Additionally, developing this technology further would include the extension of adding sensors to microneedle arrays, which will detect the condition of the patient and administer the appropriate amount of medication. After considering the development of microneedles and current innovations such as cheaper 3D printing methods and microencapsulated cell extrusion using microneedles, the aforementioned improvements must be further experimented on.

1.2.3 Pain Minimization using Microneedles

A major advantage of microneedles when compared to hypodermic needles is they are relatively painless. In “Effect of microneedle design on pain in human subjects” researchers found that while thickness, width, and tip angle did not affect patient pain, length and number of microneedles in the array did [9]. The study showed that the shortest tested length (480 um) and smallest number (5) microneedles resulted in the lowest amount of pain experienced as determined by visual analog pain scores. All pain scores indicated microneedles induced 5-40% of the pain of a hypodermic injection. Pain is also often caused by breakages upon insertion, which is usually found in glass and ceramic materials.

Relative to the range of lengths (480 -1450 um) and numbers of needles in arrays (5 - 50) tested, our device would be predicted to land on the lower end of the pain scale, with a 13 microneedle array, each 600 um long. So, according to available data on microneedle geometry’s influence on pain, our microneedles are as close as printer resolution allows to painless delivery.

This study measured pain using the visual analog pain score, which is determined by drawing a line along a ten centimeter scale, with zero indicating “no pain” and ten indicating “worst pain”. Although this is a subjective, self assessment, it has been shown to be significantly better at predicting pain than other subjective methods using digital scales.

Our device is for encapsulated cell extrusion, and infusion pressure will be monitored to determine the optimal speed to minimize pain during injection. The study “Infusion pressure and pain during microneedle injection into the skin of human subjects” found that flow rate does influence pain experienced as measured by a VAS scale once reaching a certain threshold. Similar geometry microneedles were tested at 0.1 mL/min, 0.3 mL/min, and 1 mL/min. When

delivering the final amount of saline solution at 1 mL/min, patients reported “a sharp, piercing sensation during the infusion of the last 0.2 mL, which suggests there was tissue damage,” [9].

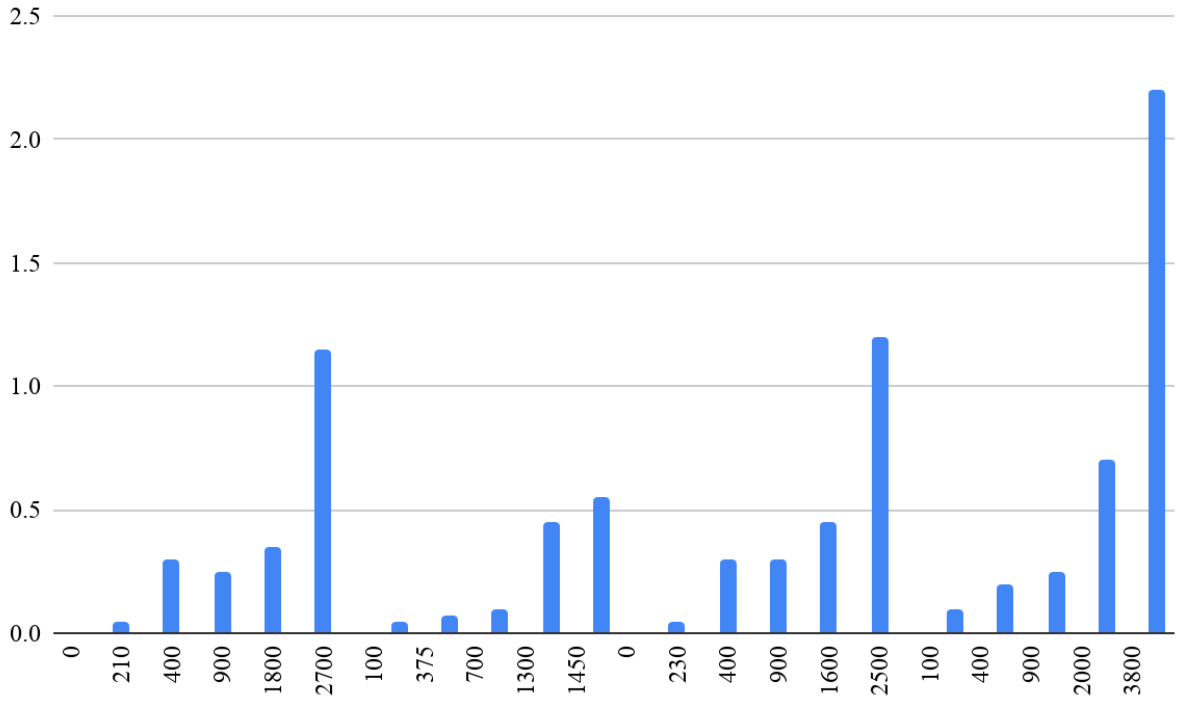

Figure 3. VAS score as a function of needle depth and injected volume [10].

Because physiological markers of pain are more reliable, these should be monitored when performing pain minimization studies.

Table 1. Physiological markers of pain used for potential parallel use in microneedle pain reduction studies.

Physiological Marker of Pain	Summary
Heart rate variability (HRV)	The key to adequate pain management is assessing its presence and severity, identifying those who require intervention and appreciating treatment efficacy. The experience of pain is complex, as reflected by its definition as “an unpleasant sensory and emotional experience, associated with actual or potential tissue damage [3].

Heart rate and blood pressure change	Cardiovascular Depth of Analgesia (CARDEAN) index has shown a correlation with noxious stimuli in intraoperative anesthesia [27].
Peripheral pulsatile component of cardiac cycle	Surgical plethysmographic index (SPI) guided drug administration during intraoperative anesthesia "resulted in reduced opioid consumption and faster recovery." In post-operative environments, moderate sensitivity and specificity was found in distinguishing the difference between low, moderate, and severe pain [27].
Electrodermal activity	Postoperative correlation between fluctuations of skin conductance (NFSC) and pain scores in adults but not children. In healthy test subjects there was correlation between heat evoked pain and NFSC, however it is unreliable due to large variability [27].
Pupil reflexes	Pupillary dilation reflex (PDR) is correlated to verbal ratir postoperative procedures [27].
EMG response	P value between brain activity and PIPP score proved positive correlation. The brain activity is stimulated primarily by a change in behavioral components (such as facial expression) rather than by a change in physiological components [28].

1.2.4 Literature Review

Recent studies on microneedle technology investigate optimal fabrication methods, materials, needle array parameters, needle geometries and morphologies. Goals of these studies include high aspect ratio to increase tip sharpness, reduced production time, and maximized needle strength. Each study proposes a specific set of characteristics for a microneedle array suiting a unique purpose.

Table 2. Studies of new applications and production methods for microneedle devices designed for transdermal drug delivery, optimal needle strength, and maximal tip resolution.

Study	Fabrication Method	Strategic Advantage	Material	Needle Characterization	Dimensions and Morphology	Aim
Simple and customizable method for fabrication of high-aspect ratio microneedle molds using low-cost 3D printing	SLA 3D printing mold fabrication ("Print and Fill" method)	Aspect ratio and tip sharpness	Carboxymethylcellulose loaded with bioresorbable Rhodamine-B	Solid	Conical shape, 5 x 5 square needle array, 1.5 mm needle to needle distance, 2.5 mm height, 625 um base diameter	Develop a print and fill method to produce high aspect ratio microneedles in a research setting.
Fabrication of hollow microneedles using liquid crystal display (LCD) vat polymerization 3D printing technology for transdermal macromolecular delivery	Liquid crystal display (LCD)	Printing resolution: 100 μm Printing angle of -52.63 degrees is optimal for penetrating the skin	NextDent Ortho rigid biocompatible resin material	Hollow	1000 μm height, 3000 μm needle-to-needle distance, 15x15 mm patch	Testing LCD to make microneedle array, compared to other fabrication methods such as SLA.
Design and Fabrication of Biodegradable Microneedle Using 3D Rapid Prototyping Printer	SLA 3D printing	High resolution on the micron scale, faster fabrication time, and high accuracy.	Four different biodegradable materials were tested: Acrylonitrile Butadiene Styrene (ABS), Polyester Resin, Polylactic Acid (PLA) and Polyvinyl Alcohol (PVA)	Solid	Conical (36π & 49π μm diameter base) and pyramidal (36×10^4 & 49×10^4 μm wide square base), 350 and 450 μm tall, single and triple microneedle patch arrays.	Conduct stress testing on variations of microneedle to identify ideal parameters and material to withstand insertion. Determined that PVA had the greatest strength. For both conical and pyramidal needles a 450 μm height, larger base area, and triple needle were ideal (withstood ~2.9 x 10^6 N/m^2 of applied stress).

Review articles summarize developments made in the field of microneedle in recent years, and compare a wide range of microneedle types. Particularly emphasized are new fabrication methods and materials.

Figure 3. Reviews of current microneedle technology.

Review	Fabrication Method	Comparison Metric	Material	Needle Characterization	Aim
Polymeric-based microneedle arrays as potential platforms in the development of drugs delivery systems	Micromilling, direct laser micromachining, chemical wet etching, electrical discharge machining, drawing lithography, UV-lithography, deep reactive-ion etching, projection-based direct light processing, fused filament fabrication (FFF) or fused deposition modeling (FDM), scanning based SLA	Resolution: micromilling, UV-lithography has higher resolution than SLA Aspect ratio: Drawing lithography has higher ratio than SLA	Silicon, glass, ceramics, dissolving and biodegradable polymers and hydrogel	Solid/coated, hollow, porous, hydrogel/swellable, merged-tip microneedles	Comparing the properties of different types of microneedles, materials and fabrication methods
3D printing as a transformative tool for microneedle systems: Recent advances, manufacturing considerations and market potential	Laser-based Stereolithography (SLA): two-photon polymerisation (2PP) Digital light processing (DLP): Continuous liquid interphase printing (CLIP)	Resolution: SLA method, specialized 2PP: nanoscale commercial laser SLA: microscale Printing time: DLP is faster than SLA	Polymeric, metallic, ceramic	Solid, hollow, biodegradable, solid ('poke and patch')	Presenting information on developing 3D printing microneedles from 2018-2021
3D printing as a transformative tool for microneedle systems: Recent advances, manufacturing considerations and market potential	Comparing Laser based SLA: two-photon polymerization and Digital Light Processing: Continuous Liquid Interphase Printing vs. conventional methods, and extrusion based printing	Printing resolution and material properties	Acrylate-based, Poly-propylene fumarate (PPF) with BAPO, Co-polymers reinforced with inorganic silanated particles, Acrylic, Methacrylate-based, Polyethylene glycol diacrylate (PEGDA) with Phenylbis, Polyethylene glycol dimethacrylate (PEG) with TPO, Polylactic acid (PLA), Sodium alginate with hydroxyapatite (HA)	Hollow, solid coated, hydrogel, biodegradable, dissolvable, solid 'poke and patch'	Summarize the field of microneedle printing by comparing printing resolution and material properties.

Microneedles: Characteristics, Materials, Production Methods and Commercial Development	Summarizing microneedle fabrication methods including: microelectromechanical systems, laser cutting, laser ablation, micromolding, atomized spraying method, droplet born air blowing method, pulling pipettes, additive manufacturing, fused deposition modelling, stereolithography, digital light processing, two-photon polymerization.	Microneedle production method and characterization.	Not listed.	Hollow, solid, solid-coated, dissolving, hydrogel	Microneedle integration into point of care and lab on a chip devices for drug delivery and diagnostic applications.
Polymeric-based microneedle arrays as potential platforms in the development of drugs delivery systems	Micromilling, direct laser micromachining, chemical wet etching, electrical discharge machining, drawing lithography, UV-lithography, Deep-reactive ion etching, projection-based direct light processing, fused filament fabrication, scanning based SLA.	Production method, material and characterization.	Ceramics, silicon, glass, dissolving and biodegradable polymers, swellable hydrogel polymers/proteins	Solid/coated, hollow, porous, hydrogel/swellable, merged tip MN.	Summarize the variety of polymer based MN applications in drug delivery.

Chapter 2 - System Level

The current design of the microneedle device structure is composed of two main parts: one containing the array of hollow microneedles, and the other consisting of a fluid chamber.

2.1 System Level Overview

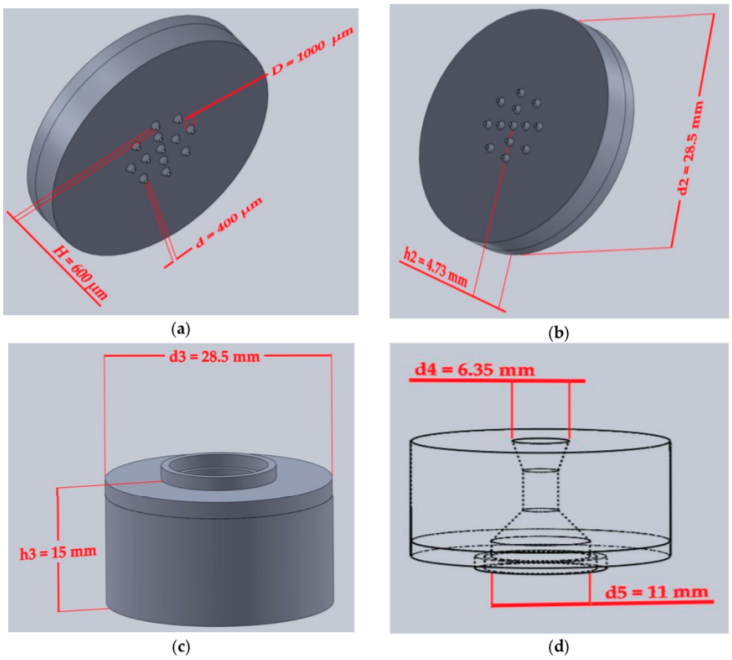

Figure 4. SolidWorks representation of the device part containing an array of conical-shaped microneedles with dimensions [5].

The bottom component of the device modeled in Figure 4 is a circular array of 15 conical-shaped hollow microneedles, organized in a circular fashion. The dimensions of the cones are: 600µm in height, a large opening diameter of 1,000µm, and a tip diameter of 400µm. The openings of the hollow microneedles traverse through the part to the opposing surface, forming a hole for each microneedle. The flat surface of this part will be glued to the larger circular surface of the fluid chamber part. The fluid chamber is 15mm in height and 28.5mm in diameter. The opening where the syringe will be loaded for injection has a diameter of 6.35mm and the larger circular surface of the fluid chamber that will connect to the microneedle array is 11mm in diameter. This piece serves as a fluid chamber to contain the liquid and cells dispensed by the syringe and is the bridge that connects the syringe tip and the microneedles.

2.2 Materials

3D Printing Protocol

There are several methods of 3D printing microneedles, which use either direct or indirect printing. These methods include stereolithography (SLA) and digital light processing (DLP), where direct printing is the creation of microneedles to create the device, and indirect printing is used to make a mould for the microneedles. Our design uses laser stereolithography (SLA) to directly print hollow microneedles that protect microencapsulated cells from shear stress. Recent literature explains that improvements within photopolymerization and extrusion-based 3D printing depend on enhancing printing resolution and identifying the best material to confer the desired material properties [22]. Our 3D printed microneedles are made out of Formlabs Clear photoresin which is then printed using a Formlabs 2 printer. The liquid photoresin is a plastic composed of short carbon chains that contains the necessary components of a final solid plastic before polymerization. The SLA 3D printer uses UV light to cause the chains of the molecules to link to form long and stiff carbon chains. When enough carbon chains link, they form a solid plastic that makes up the 3D printed material of the microneedle device. The process of polymerization of the carbon chains is demonstrated in figure 5.

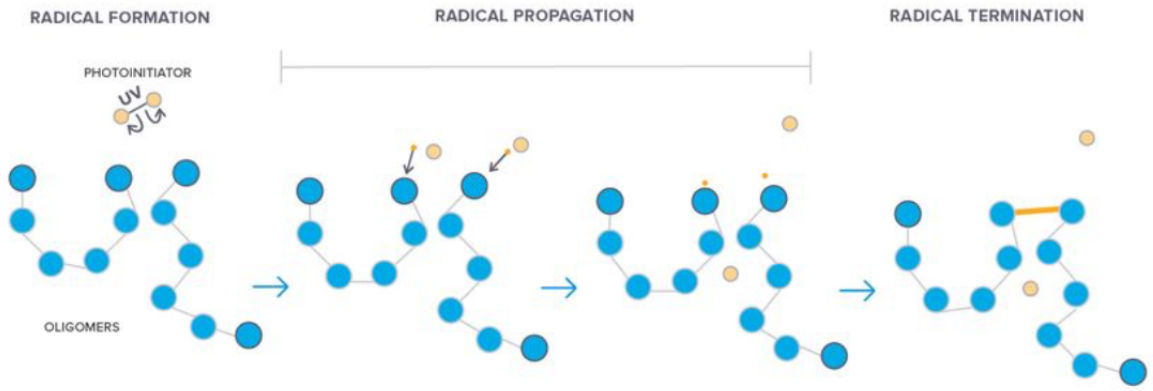

Figure 5. Steps of Polymerization [6].

We were not granted access to the lab and were not able to utilize the SLA Formlabs Form 2 printer. Due to this protocol, we modeled our device on SolidWorks and focused on using Multi-physics software to generate predictive profiles of biologic delivery pre-puncture.

2.3 Methods

This section will discuss the methods used to simulate laminar flow and particle trajectory through the microneedle device. 2D and 3D interior geometries (Figure 6) were created in COMSOL for analysis. This allows for modelling of the liquid extruded through the device directly rather than as a liquid filling.

The COMSOL Simulations were performed using COMSOL Multiphysics Version 5.5.

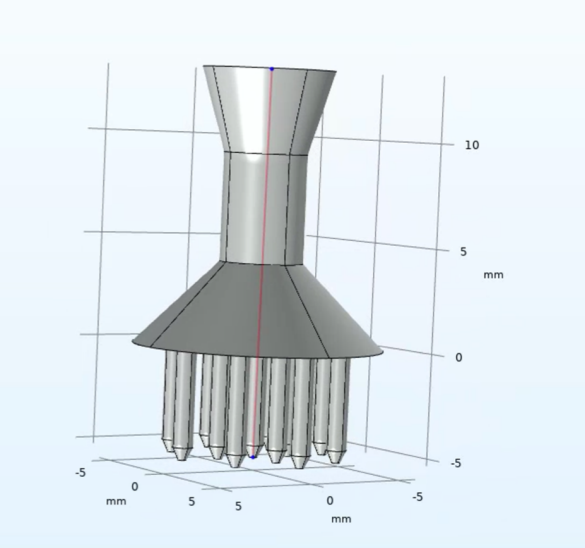

Figure 6. Center of microneedle device modeled as a solid for COMSOL simulations.

2.3.1 Laminar Flow Model

COMSOL was used to model laminar flow through the microneedle device to predict the flow profile of solution upon extrusion. The Laminar Flow Interface on COMSOL is used primarily to model flow at small to intermediate Reynolds numbers. The physics interface for single-phase fluid flow is based on the Navier-Stokes equations.

Navier Stokes Equations

The Navier-Stokes equations govern the motion of fluids. These equations can be seen as Newton's second law of motion for fluid flow. For a incompressible Newtonian fluid, the equations are the following:

$$\rho(u * \nabla)u = \nabla * [-\rho l + K] + F \, [1]$$

$$\rho\nabla * u = 0 \, [2]$$

$$K = \mu(\nabla u + (\nabla u)^T)[3]$$

where u is fluid velocity, p is fluid pressure, ρ is fluid density, and μ is fluid dynamic viscosity. F is the volume force vector and K is zero because our flow is non-viscous and incompressible. Equation 1 is a vector equation which represents conservation of momentum and Equation 2 is the continuity equation that represents the conservation of mass.

Simulation Parameters

Laminar flow was modelled through the device using the same dynamic viscosity and fluid density as water: 8.90 Pa*s and 997 kg/m^3 respectively. Inlet velocity was set to 1.58x10^{-4} m/s, equivalent to that of 0.3 mL/min which falls in the therapeutic range for pain minimization.

2.3.2 Particle Trajectory Model

In order to visualize the flow of microencapsulated cells through the device, we ran a time-dependent particle trajectory using the Particle Tracing Module on COMSOL. This module is a general-purpose tool for computing the paths of particles as they travel through a geometry and are subjected to various forces. The simulated particles in our study represent microencapsulated cells that would be extruded through the device. Their trajectories are computed in the time domain by solving a set of equations based on Newton's Second Law of Motion, to which the forces based on external fields can easily be added.

Drag Force

For laminar flow, the drag force contributes to the advective transport of the particles. The drag force equation is as follows:

$$F_d = \frac{1}{\tau_p} m_p(u - v) \text{ [4]}$$

The equation is based in Stokes Law, as the particles are small enough that the flow remains laminar with a Reynold's number below 2300, while Schiller-Naumann's equation would be used for turbulent flow with a higher Reynold's number. F_d represents the drag force, or friction force acting at the interface of the fluid and particles, while u and v are the velocities of the particle and fluid respectively.

Simulation Parameters

The particles in our simulation have a diameter of 300 microns. The particle density is 1178 kg/m^3, and the particle charge was set to zero. The boundary condition is the freeze boundary which stops the particles when they hit a wall. The release condition is mesh based where the particles are released from within each mesh element. This release condition best simulates a syringe extruding the cells into the device.

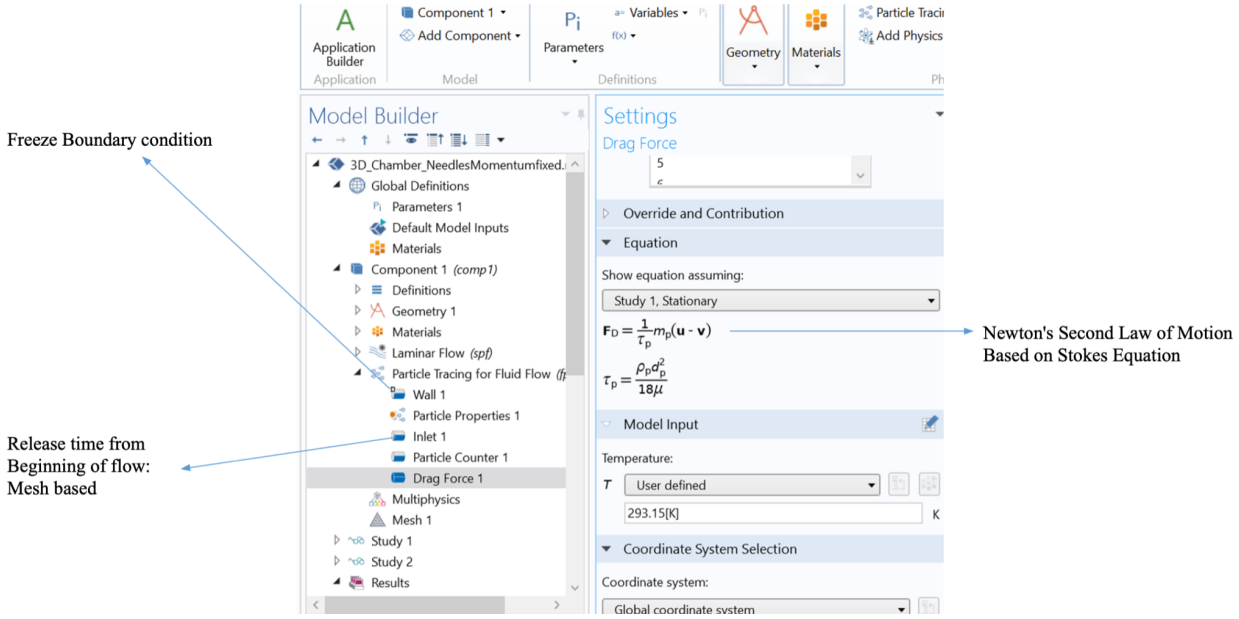

Figure 7. Equations and Conditions for COMSOL Particle Trajectory

2.3.3 Failure Mode Analysis

Several failure modes were modeled including: clogged nozzle, deformed needle tip, and suction. By creating potential defected geometries, velocity, pressure, and particle tracing plots can be generated to determine the effect of the different failure modes. Then, by ranking the negative effect of each failure mode, the processes will be addressed in order of descending risk priority number. The risk priority number will be calculated using the equation below.

$$RPN = Sev * Prob * Det \quad [5]$$

2.4 Benchmarking Results

There have been various studies that have designed similar transdermal microneedle delivery systems for drugs [10],[21]. However, there is only one study that has developed hollow microneedles as a delivery system for cell therapy [7]. The study extruded non-cultured epidermal cells (NCECs) through silicon hollow microneedles and observed positive NCECs viability results; in addition, some of the injected NCECs maintained their function in *ex vivo* human skin [7].

This study deviated from our project as they fabricated their microneedles using photolithography [10],[21]. No other study has attempted to use 3D printing as their microneedle structure fabrication method making this project a novel development.

2.5 Key System Level Issues

The primary issue in our system is the reliability of software and simulations. There will potentially be a discrepancy between our calculated results and simulated results. The significance of this discrepancy needs to be experimentally determined with respect to the shear on the microcapsules for optimized validation.

2.6 Bernoulli's Equation and Continuity Equation

The following equation relates the flow rate (Q), in m^3 per second to velocity (v), in m per second and area (A), in m^2. The initial flow rates were 0.3, 1.2 and 12 mL/minute, which were converted to m^3 per second. After using the equation the initial velocities were found and used in the continuity equation.

$$Q = v * A \quad [6]$$

The continuity equation relates the change in velocity to the change in area as the mass is conserved (shown below). This is necessary as the diameter of the device changes through the initial chamber, the larger reservoir chamber, the input of the microneedle, and the output of the microneedle.

$$v1 * A1 = v2 * A2 \; [7]$$

The following figure shows the geometry of the microneedle device, with the various diameters used in calculations.

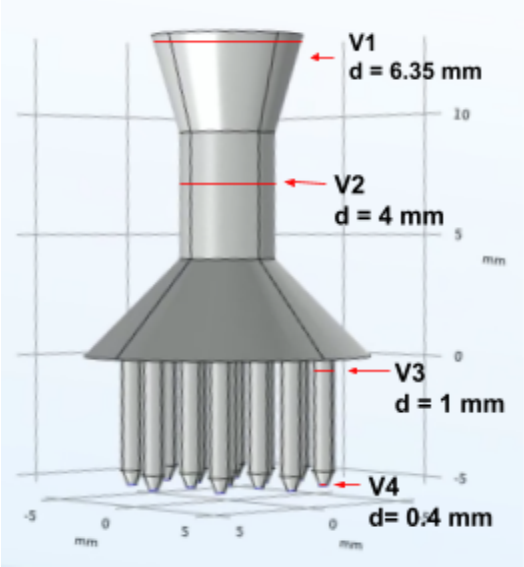

Figure 8. Velocity samples collected at four different locations for 0.3, 1.2, and 12 mL/min flow rates.

Bernoulli's equation relates the change in pressure to the change in velocity found from the continuity equation. The following equation was used, with initial pressure set to the value used in COMSOL, density (ρ) set to the density of water, height (Z) changed based on the device geometry, and area and velocity used from the previous equation.

$$\frac{p1}{\rho 1} + g * Z1 + \frac{A1*v1^{2}}{2} = \frac{p2}{\rho 1} + g * Z2 + \frac{A1*v2^{2}}{2} [8]$$

2.7 Team and Management

Our team is composed of three student members and our advisor. We maintained weekly communication since the founding of our group and project. Our project is a continuation of a project created in 2018 under the supervision of our current advisor. We utilized a Google Drive folder to collect our research and collaborate on simulations, MATLAB code, and literature reviews. Weekly meetings were set up with our advisor to ensure productive progression of the project. All members were trained and proficient in Solidworks, COMSOL, and MATLAB.

2.8 Risks

Due to our project being entirely virtual, we have no health or material risks. The main risk we have in our design project approach is having discrepancies in reality versus simulations. Our simulations will generate predictive models of the flow profile of the device, however the significance of these potential discrepancies needs to be experimentally determined.

2.9 Timeline

Fall 2020	**Winter 2021**	**Spring 2021**
❏ Outline goals for project ❏ Budget and funding ❏ Literature review ❏ COMSOL Simulations of fluid mechanics and flow rate	❏ 3D print microneedles using Maker Lab ❏ Verify that previous results can be replicated ❏ Test reliability of needles using flow modeling ❏ Perform pressure analysis to minimize pain ❏ Create a larger-scale model ❏ Model/monitor cell extrusion efficacy	❏ Finish results analysis ❏ Write thesis report ❏ Publish our findings ❏ Prepare our senior design conference presentation

2.10 Cost Analysis

Item	Vendor	Cost
COMSOL Software Package	NA	School Of Engineering
MatLab Software Package	NA	School Of Engineering
3D Printing Materials and Labor	SCU Maker's Lab	$200.00
Scanning Electron Microscopy/ Atomic Force Microscopy	SCU CNS	$600.00
Pressure sensitive paper		$299.00
NIST Particles		$365.00
Blue Dextran dye	Sigma Aldrich	Department of Bioengineering
Biopolymers	N/A	Department of Bioengineering
Disposables (1 mL syringes)	Thermo Fisher	Department of Bioengineering
syringe pump	New Era	Department of Bioengineering
Camera	Biomomentum	Department of Bioengineering
Sterilization	NA	Department of Bioengineering
Cell culture	NA	Department of Bioengineering
		$1,464.00

Chapter 3 - Subsystems Level

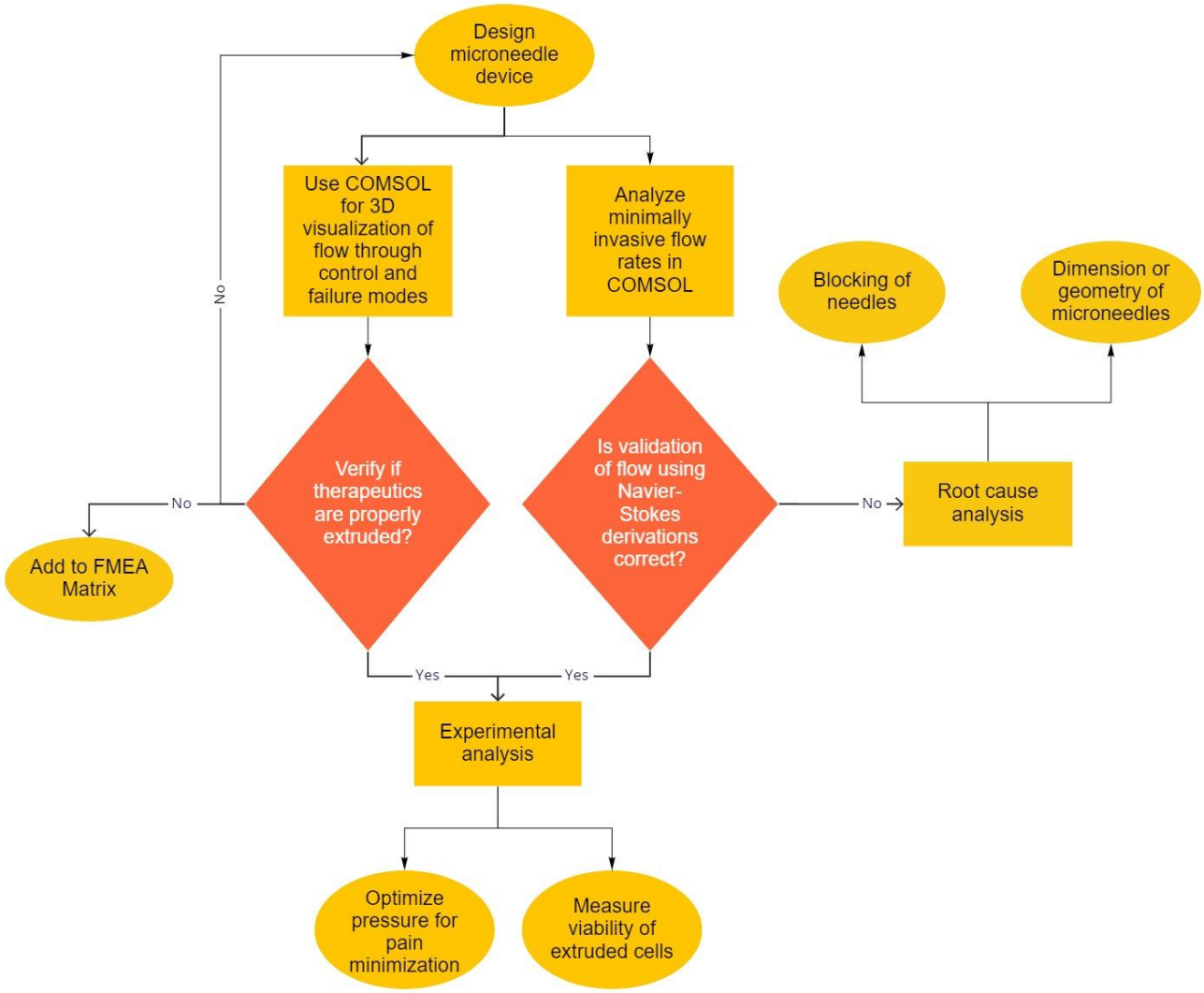

Figure 9. Subsystems flowchart.

Chapter 4 - Simulation Results and Discussion

The purpose of this chapter is to present the results for the studies that we performed in COMSOL. These simulations developed a flow profile for the custom microneedle device. We tested a single-phase stationary laminar flow and time-dependent particle tracing through fluid flow through our validated model. We also tested three different failure models using our device to evaluate their effect on the flow profiles. The three failure models are a clogged nozzle, a disformed nozzle, and suction.

4.1 Flow Profiles

4.1.1 Study 1: Stationary Laminar Flow

As stated previously, the conditions of the laminar flow are as follows:

Dynamic Viscosity: 8.90×10^{-4} Pa·s

Density: 997 kg/m³

Inlet Velocity: 1.58×10^{-4} m/s

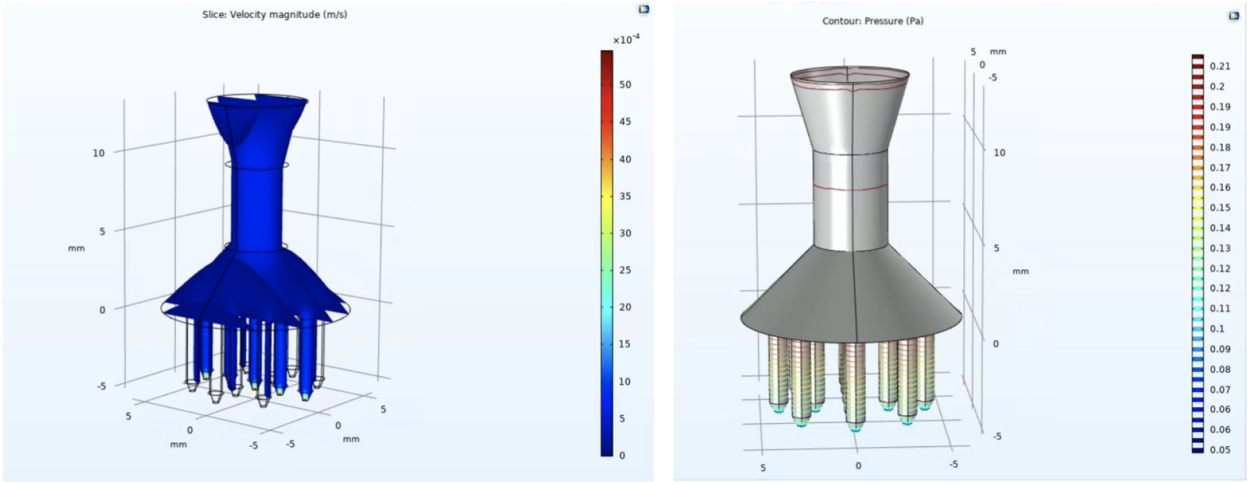

(a) (b)

Figure 10. COMSOL results graphs. (a) Slice plot of velocity magnitude for laminar flow (m/s). b) Contour pressure plot for laminar flow (Pa).

The outlet velocity through the 13 nozzles is about 5.3×10^{-3} m/s. The pressure through the 13 nozzles is about 0.08 pascals. This outlet velocity is optimal for pain minimization based on Gupta et. al.'s study on flow rate as discussed in Chapter 1.1. To verify the force of the flowrate pre-puncture, we modeled the impact force through the nozzles using the impact force equation. The impact force through the nozzles is about 2.1×10^{-10} newtons.

$$IF = \rho v^2 A \text{ [9]}$$

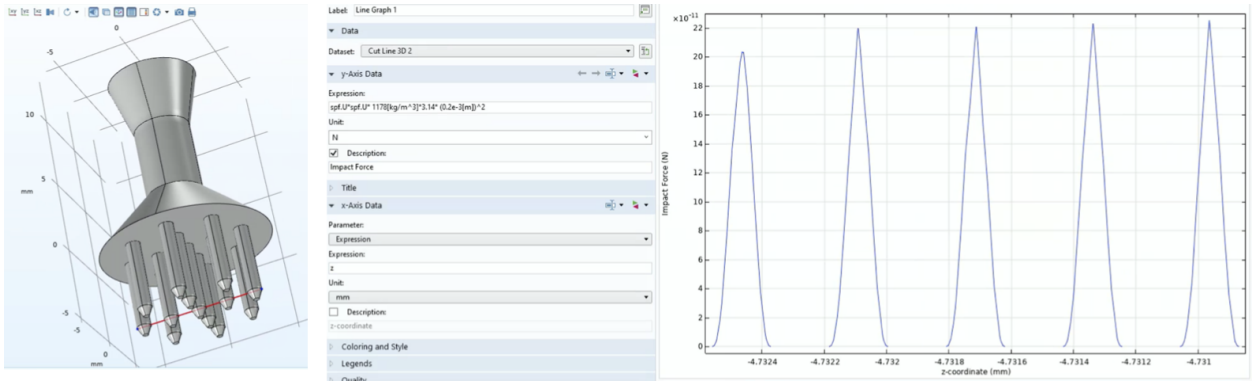

(a) (b)

Figure 11. (a) Cut-line across device to calculate impact force is located across five nozzles at the beginning of the needle. (b) Graph of impact force across five needle in Newtons

4.1.2 Study 2: Time-Dependent Particle Trajectory

As stated previously, the conditions of the particle trajectory are as follows:

Particle diameter (dp): 300 μm

Particle density (ρ): 1178 kg/m^3

Charge number: 0

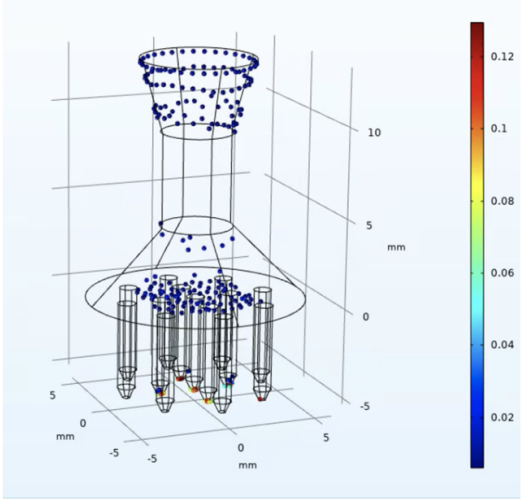

Figure 12. Particle Tracing plot at 2 seconds

The particle trajectory image is captured at 2 seconds post particle injection. The image demonstrates the particles flowing through the device and traveling down the needles' chambers. The particles seen stationary at the top of the device are a result of the wall freeze condition set

by COMSOL. The color scale on the right of Figure 12 represents the particles' velocities in meters per second; the fastest particles are congregated in the needle tip, and the slowest particles are either cemented to the boundary or halted at the base of the device. The flow of particles enters the center nozzles at a faster rate than the outer nozzles as a result of the cone-like geometry. This is to slow the velocities of the particles through the device to maintain a therapeutic flow rate for pain minimization.

4.2 Failure Models

4.2.1 Clogged Nozzle

The first failure mode we investigated is a clogged nozzle. This failure may occur due to microcapsule aggregation that is strong enough to halt particle and fluid flow through the needle tip. Clogging may also occur due to a printing defect such as nozzle shrinking below the designed 400 micron diameter. This type of 3D printing defect may occur as a result of deficient polymerization. When the printer inadequately polymerizes the resin from a liquid to a solid, the structural integrity of the microneedle tip is compromised. Finally, the encapsulation of the mammalian cells may not be uniform, resulting in microencapsulated cells with a diameter greater than 300 micron. As a result of uneven size distribution, the microencapsulated cells may be too large to pass through the needle, resulting in a clogged nozzle.

In COMSOL, we modeled a clogged needle by deselecting either one nozzle, or several nozzles as an output option in the laminar flow module. Figure 13 shows the results of the center theoretically clogged.

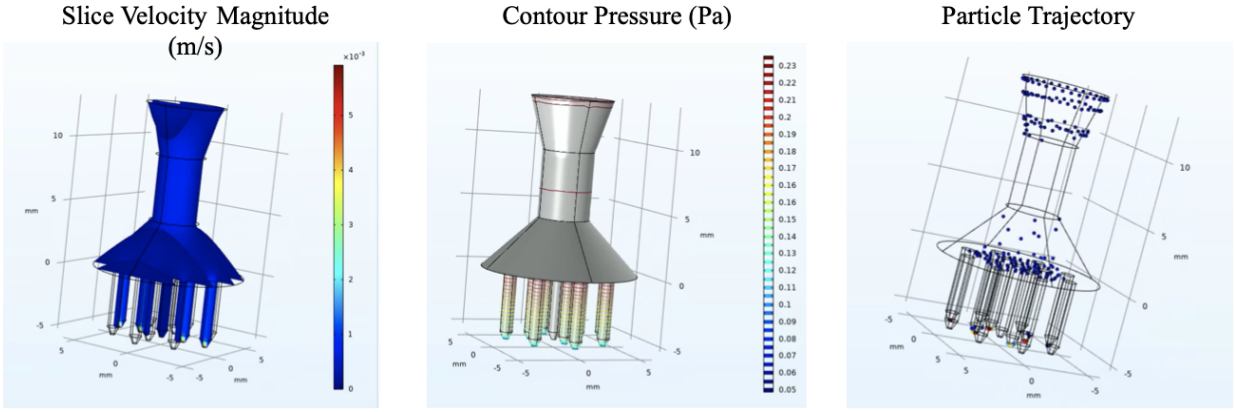

Figure 13. Velocity, pressure, and particle trajectory plots demonstrating the center nozzle as clogged

By clogging the center nozzle, the remaining nozzles who still experienced flow have an increased outlet velocity of 5.5×10^{-3}m/s and a pressure increase from 0.08pa to 0.09pa. As there was no laminar flow through the center nozzle, no particles traveled through the needle chamber.

This is a discrepancy from what one may expect in the lab as the particles may have been the cause for the clogged nozzle and would therefore appear in a particle trajectory plot.

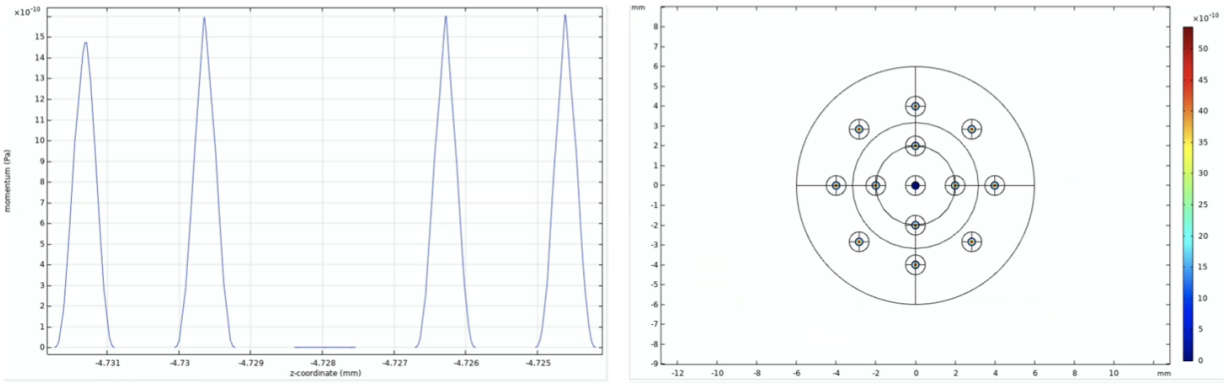

(a) (b)

Figure 14 . (a) One dimensional graph of Impact force plot of 5 needles with center needle clogged. (b) Plane plot of impact force of all 15 needles with center needle clogged.

The impact force through the clogged nozzle is zero which has logical integrity as there is no flow traveling through the needle tip, and therefore no velocity at the point of measurement. The impact force of the surrounding nozzles increased to about $15x10^{-10}$ N as they experienced a higher velocity as a result of the clogged nozzle.

To prevent the occurrence of this failure mode, clogged nozzle provisions should be in place. Before encapsulation of the cells, one should explore the use of surface coating to reduce the chance of particle aggregation. This may be done by giving the particles a charge to reduce their probability of sticking together. During testing, one should implement a design method to visually inspect the microneedles under a microscope to capture clogging. After testing, one may also reoptimize the parameters for the atomization processes and reinforce microscope inspection prior to infusion of microcapsules into the device.

4.2.2 Deformed Nozzle

The second failure mode we investigated is a deformed needle tip. This particular failure mode could occur in the lab due to denting of the tip as a result of a shortened washing step post 3D printing. The washing step is critical to remove all non crosslinked polymers present in the device. If this step is not performed properly, then the 3D printed microneedles have the risk of being disformed. The material that makes up the device is brittle in nature and is at high risk of experiencing a random fracture that could disrupt the uniformity of the device. Deformation may also occur due to a CAD defect if the device is not modeled properly.

One way in which the deformed nozzle was modeled in COMSOL is by shrinking the needle tip from 400 microns to 200 microns which is most likely to occur due to a CAD defect.

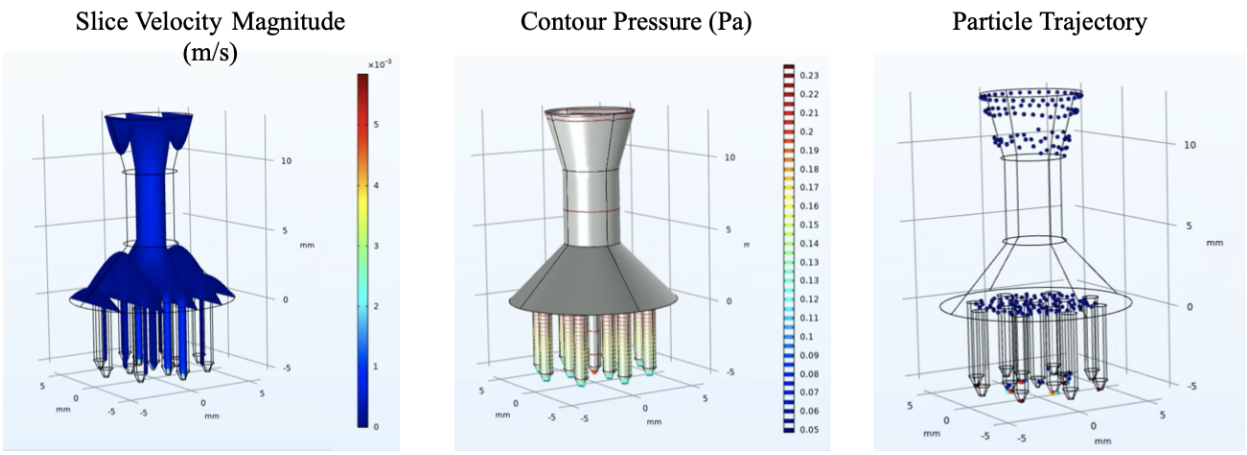

(a) (b) (c)

Figure 15. Velocity, pressure, and particle trajectory plots demonstrating a disformed center needle from 400 microns to 200 microns in diameter.

When the center needle was shrunk to 200 micron, its velocity experienced a decrease from $5.3x10^{-3}$ m/s to $4.0x10^{-3}$ m/s. The nozzles that did not undergo deformation had an increased velocity of $5.5x10^{-3}$m/s. The pressure of the deformed nozzle increases to 0.20 Pa and the un-changed nozzles slightly increase to 0.09 Pa in comparison to the control experiment which has a pressure of 0.08 Pa. Particles still traveled to the deformed nozzle, however, congregated at the base of the nozzle as they are too large to pass through.

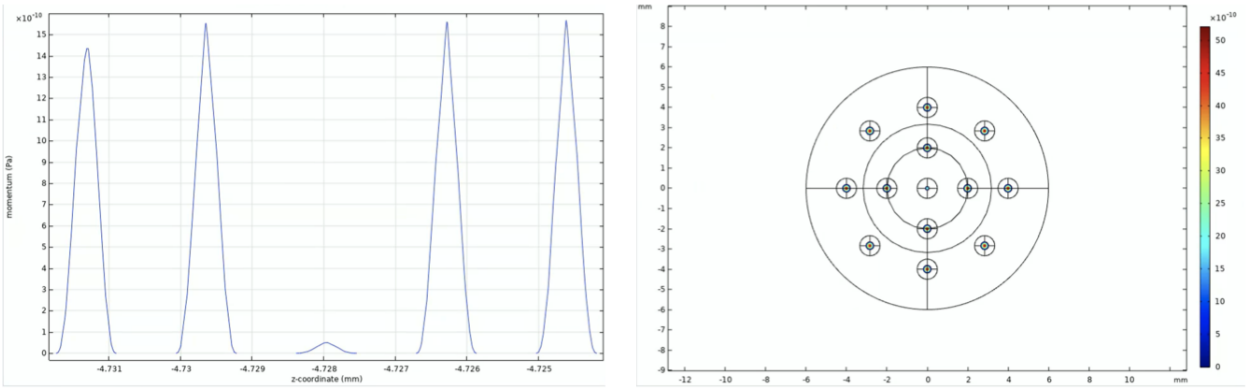

(a) (b)

Figure 16. (a) One dimensional graph of impact force plot of 5 needles with center nozzle deformed. (b) Plane plot of impact force of all 15 needles with center nozzle deformed.

The impact force of the unchanged nozzles increased from $2.1x10^{-10}$N to $14.5x10^{-10}$N while the deformed nozzle's impact force was $3x10^{-11}$N. The center nozzle has a decreased impact force because the velocity is lower in the deformed tip as it has a smaller cross sectional area for the flow to travel through. Since less fluid can travel through the deformed tip, the remaining needles will experience a higher velocity of fluid flow and therefore have a greater impact force.

To prevent the occurrence of this failure mode, deformed nozzle provisions should be in place. One provision is to increase the wash time after cross-linking the device's photo resin to guarantee a smooth transition from liquid resin to solid resin. Another provision is to design a visual inspection under the microscope to investigate a deforemd nozzle as well as design a Charpy test for the microneedles. Finally, the handler should always revise the CAD design before submitting the device plans to the 3D printer.

4.2.3 Suction

Suction is used to sample microcapsules for quality as a routine test prior to therapeutic use. If the vacuum palette is uneven, the force will be applied heavily to a single nozzle. The additional shearing of the capsules may cause cellular damage and result in an inaccurate sample of extruded microcapsules, rendering the suction test non functional.

Suction was modeled in COMSOL by setting the pressure of the nozzle experiencing suction to -500 Pa while keeping the remaining nozzles at 0 Pa. Figure 17 denotes the center nozzle experiencing suction.

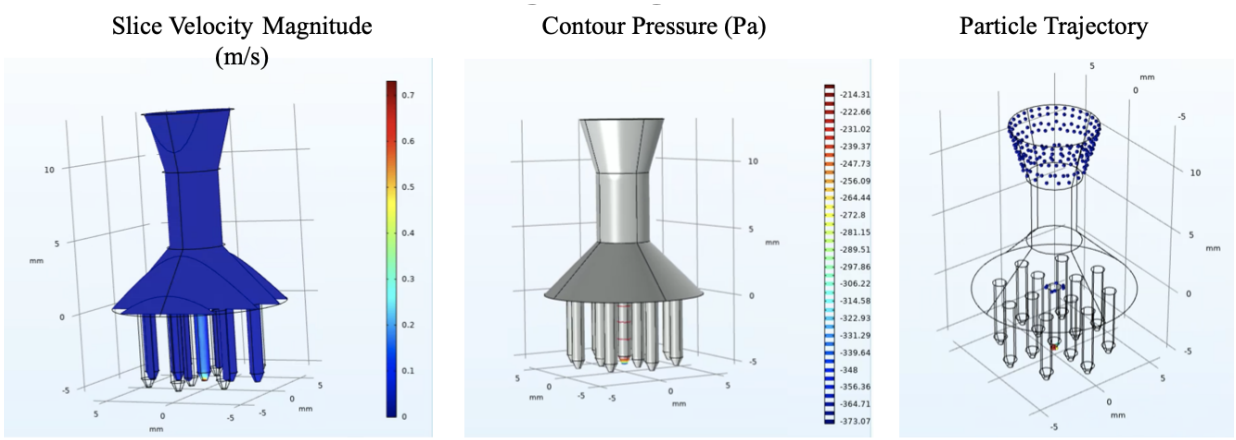

(a) (b) (c)

Figure 17. Velocity, pressure, and particle trajectory plots demonstrating suction on the center needle with an outlet pressure of -500 Pa.

The center nozzle undergoing a pressure of -500 Pa, experienced a velocity of 0.7m/s. This is almost three times the magnitude of the control laminar flow experiments and is due to the significant pressure difference experienced by this nozzle compared to previous experiments. The remaining nozzles experience a velocity of 0.05 m/s. The pressure of the center nozzle post laminar flow is -300 Pa while the remaining nozzles have a pressure of 0 Pa. As a result of this uneven pressure distribution, the only particles that were traced for the particle trajectory plot are at the nozzle tip of the center nozzle, at the base of the center nozzle, and at the top of the device.

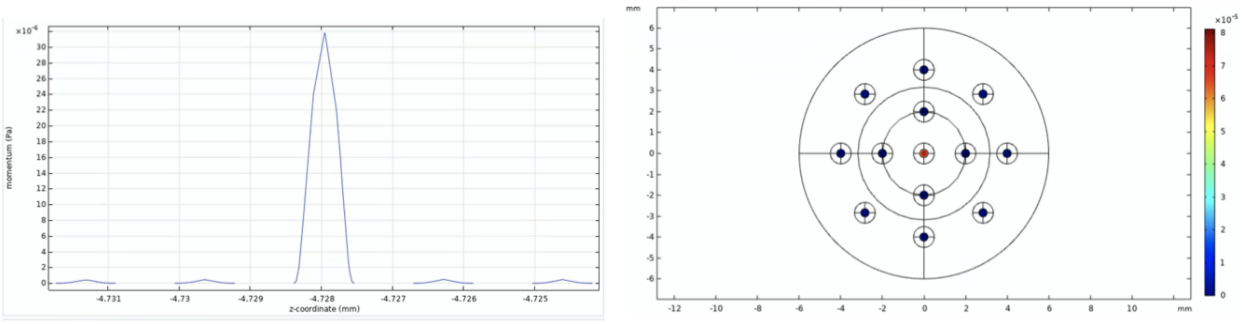

(a) (b)

Figure 18. (a) One dimensional graph of Impact force plot of 5 needles with center nozzle experiencing suction. (b) Plane plot of impact force of all 15 needles with center nozzle experiencing suction.

The impact force of the center nozzle is 3.2 x10^{-5}N while the remaining nozzles are about 2x10^{-7}N. Pressure does not directly affect impact force, however, the center nozzle is experiencing a greater impact force than the other nozzles due to ite higher velocity inside the nozzle. In the case where suction was not applied (control), the value of the impact force was 2x10^{-10}N. The values differ by 3 orders of magnitude suggesting that suction does affect the neighboring nozzles. However, the significance of this discrepancy needs to be experimentally determined with respect to the shear force on the microencapsulated cells.

Designing a vacuum palette to sample from the nozzles evenly will allow the suction to be incorporated into our workflow as a provision for routine microcapsule integrity and cell quality monitoring.

4.3 Flow Verification

In order to ensure that COMSOL derived values for impact force and output nozzle pressure were plausible, Matlab was used to calculate expected velocities derived from the Bernoulli's and Continuity equations.

4.3.1 Laminar Flow

The first step in validating the model is checking that the observed flow is laminar. Bernoulli's equation and the continuity equation, which will be later used to evaluate our theoretical model, rely on laminar flow conditions. In cylindrical ducts, such as microneedle shafts and the connected reservoir, Reynold's number should be below 2300 to qualify as laminar flow. Table 4 below shows the mean Reynold's number calculated for each of the tested flowtates, all well below the threshold.

Table 4. Calculations of the mean Reynold's number at each flowrate to ensure that flow is laminar.

Input flow rate (mL/min)	Mean Reynold's number
0.3 mL/min	2.6768
1.2 mL/min	10.7074
12 mL/min	107.0737

Laminar flow varies throughout the device and peaks at areas of stagnation, which were detected by plotting Reynold's number vertically down the center of the device, as illustrated in Figure X. Stagnation peaks at 4.73 mm and 15 mm, the two areas where the device suddenly narrows.

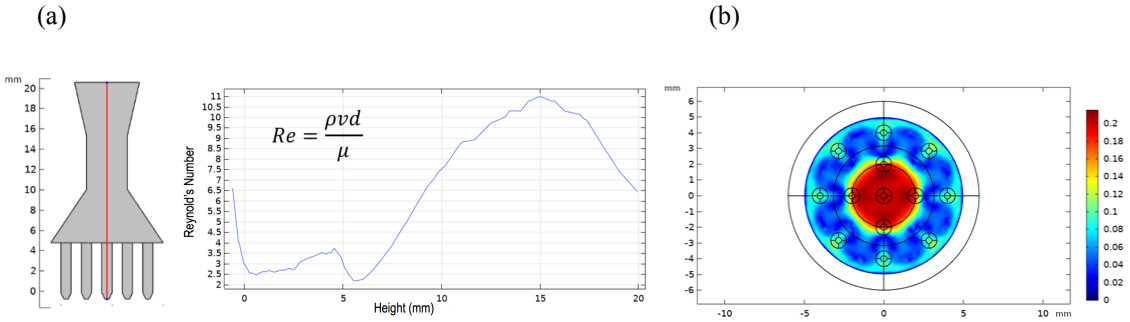

Figure 19. (a) Reynold's number plotted as a function of height in millimeters through the center of the device. (b) The stagnation zone detected in Plot A at height 4.73 mm.

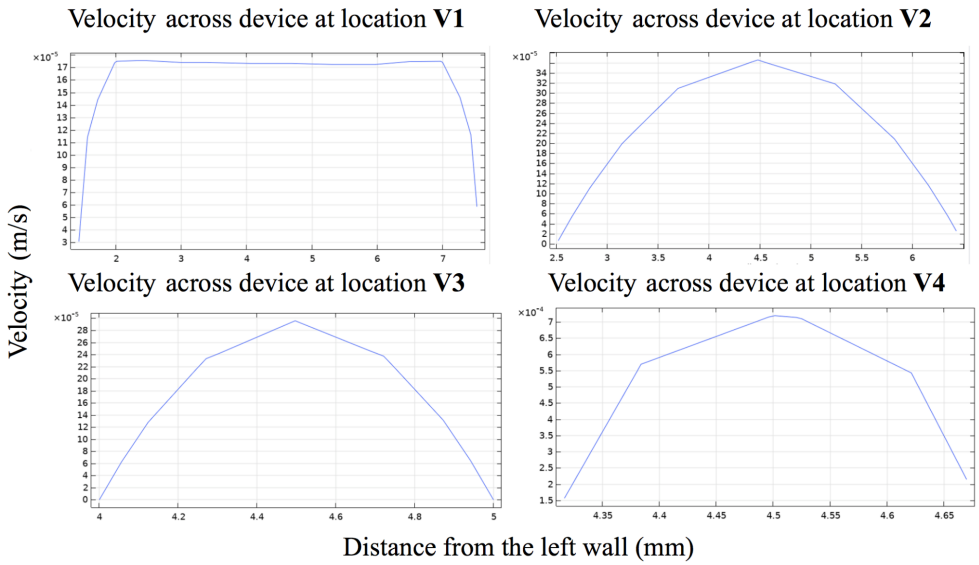

Figure 20. Velocity profiles across horizontal cutlines at locations V1-V4 as specified in Figure 8.

These flow profiles demonstrate how velocity varies across the diameter of the cylinder at each of our four locations. The V1 profile is based on the uniform input flow rate, therefore the velocity profile is relatively uniform across the diameter. The other three velocity profiles show the fastest velocity is at the center of the cylinder at each location.

- Location 1: The flow is not fully developed. Entrance effects need to be taken into consideration by the theoretical model.
- Location 2: The flow is displaying an entrance region profile. In addition, there is the discrepancy as a function of a cumulative error from location 1.
- Location 3: The flow is past a stagnation zone and is not fully developed, displaying an entrance region profile. There also is also a cumulative error resulting from the steps above.
- Location 4: The flow is fully developed. The discrepancy is a result of a cumulative error.

4.3.2 Theoretical vs. Simulated Fluid Velocity

Velocity was sampled at four locations within our COMSOL model; V1 is the entrance velocity, V2 is the velocity as the reservoir narrows, V3 is the velocity as the fluid enters the microneedle shaft, and V4 is the final velocity as the fluid is extruded. These locations were selected because they represent the four different zones of the device, each with a unique diameter. The corresponding theoretical velocity values were generated using the continuity equation. They were calculated at all three of our tested flow rates. The theoretical values for the flow rate of 0.3 mL/min are compared with their corresponding COMSOL sample values in the table 5. The velocities have the same order of magnitude, but the discrepancy between the values increases from top to bottom.

Table 5. Comparison of theoretical and COMSOL derived velocities at each location specified in Figure X for an initial flow rate of 0.3 mL/min.

Location	Theoretical Velocity (m/s)	COMSOL Velocity (m/s)
V1	1.5788×10^{-4}	1.5922×10^{-4}
V2	3.9789×10^{-4}	3.5972×10^{-4}
V3	4.8971×10^{-4}	2.8546×10^{-4}
V4	3.0607×10^{-3}	5.3467×10^{-3}

Table 6. Comparison of theoretical and COMSOL derived velocities at each location specified in Figure X for an initial flow rate of 1.2 mL/min.

Location	Theoretical Velocity (m/s)	COMSOL Velocity (m/s)
V1	6.3158×10^{-4}	6.4875×10^{-4}
V2	1.5915×10^{-3}	1.4183×10^{-3}
V3	1.9588×10^{-3}	1.1193×10^{-3}
V4	1.2243×10^{-2}	2.1681×10^{-3}

Table 7. Comparison of theoretical and COMSOL derived velocities at each location specified in Figure X for an initial flow rate of 12 mL/min.

Location	Theoretical Velocity (m/s)	COMSOL Velocity (m/s)
V1	6.3153×10^{-3}	6.3783×10^{-3}
V2	1.5915×10^{-2}	1.3686×10^{-2}
V3	1.9588×10^{-2}	1.1566×10^{-2}
V4	1.2243×10^{-1}	2.1370×10^{-2}

When examining why discrepancies accumulate as fluid moves downward through the device, a modified version of Bernoulli's equation was created which takes into account the work done by the syringe pump required to move fluid into the reservoir, and the heat lost due to friction as the fluid moves through the device.

$$\frac{p_1}{\rho} + gz_1 + \frac{v_1^2}{2} + W_{pump} = \frac{p_2}{\rho} + gz_2 + \frac{v_2^2}{2} + h_{friction} \quad \text{[Equation 9]}$$

p_1: Input pressure (Pascals)
ρ: Density of the fluid (kg/m^3)
g: Acceleration due to gravity (m/s^2)
z_1: Upper height (meters)
W_{pump}: Work to pump fluid through device ($kg*m^2/s^2$)
p_2: Output pressure (Pascals)
z_2: Lower height (meters)
$h_{friction}$: Loss due to friction in needle tip ($kg*m^2/s^2$)

Although possible that the work and friction terms could have cancelled out, this was not the case and thus errors accumulated within the device.

Table 8. Calculations of each term in Equation 9 in order to identify the sources of discrepancy between our theoretical and experimental velocity values.

	TOP (Device)			**BOTTOM (Nozzle)**
p/rho	0.00002781		p/rho	0
$v^2/2$	1.2482E-08		$v^2/2$	0.000000245
gz1	0.19943		$h_{friction}$	0.026579592
W_{device}(J/s)	0.172877986			
mass flowrate (kg/s)	0.000005			
W_{device}(W)	9.00E-07			
	TOP (Nozzle)			BOTTOM(Nozzle)
p/rho	0.0000128		p/rho	0.000009
$v^2/2$	2.4642E-08		v^2/2	0.000000125
gz1	0.00588		$h_{friction}$	0.000783673
W_{device}(J/s)	0.0058837			
mass flow rate (kg/s)	0.000001			
W_{device}(W)/nozzle	6.00E-09			

4.4 Failure Modes and Effects on Analysis

The failure modes and effects analysis (FMEA) matrix is used to identify various possible modes of failure in a design. The overall risk of failure is calculated using three components: the severity, probability, and detectability of failure. Each of these components is rated on a scale of one to ten, with one being the most ideal, and ten being the least ideal. The risk priority number (RPN) is calculated by multiplying these three values, which is shown in the table above. The table has been split into three sections, first, the process FMEA encompasses possible failures in design, manufacturing, and assembly before the device is distributed to the intended users. Secondly, the user FMEA which encompasses possible failures attributed to the user improper use of the device. Lastly, the COMSOL-based FMEA which encompasses the failure modes modeled in COMSOL that could be simulated due to improper geometry and particle-related errors. The matrix is ordered in descending order, from highest RPN to lowest RPN as the item

with the highest number requires the most attention. In the FMEA, the current design control is listed to explain how the developers are reducing the probability value, however, modes of failure that did not have a current design control were given one in the “recommended actions” column. By creating the FMEA we created a crucial component to identify and improve reliability issues of the device. The corresponding tables are shown below.

Table 9. Process-based Failure Modes and Effects Analysis

Item / Function	Potential Failure Mode(s)	Potential Effect(s) of Failure	Sev	Potential Cause(s)/ Mechanism(s) of Failure	Prob	Current Design Controls	Det	RPN	Recommended Action(s)
Cell culture for microencapsulated cell therapy	Contamination of cells	Unsterile therapeutic	9	Unsterile culturing techniques	8		3	**216**	Check cells when culturing and during assay
Stereolithography 3D printer	Inability to produce proper resolution	Increase in patient pain due to inaccurate device dimensions	6	Malfunctioning of 3D printer	5	3D printer testing	5	**150**	
Solvent sterilization	Incorrect solvent mixture, incorrect percentage of ethanol	Unsterile device	9	Manufacturer error	2		7	**126**	Routine sterilization to resolve sterility issues not compliant with standard sterility assurance level (SAL)
Microneedle array drawing in SolidWorks	Inaccurate design dimensions	No puncture of increase of pain when puncturing due to incorrect device dimensions	7	3D printer user error	4		4	**112**	Routine 3D printer accuracy testing. After printing, measure dimensions of microneedles using a micrometer screw gauge.
Flow rate of microcapsules	Inaccurate flow rate	Patient's pain is increased, drug is not delivered at flow rate used for pain minimization	4	Malfunctioning of syringe pump	5	Syringe pump testing	4	**80**	Design more extensive syringe pump testing methods
13 Microneedle Nozzles	Blockage of nozzle tip	Drug will not be dispensed equally across all 13 nozzles	5	Aggregation of microcapsules	5	Clean using air pump between runs, visual inspection of 13	3	**75**	

						microneedle array			
Stereolithography 3D printer	Tapering of microneedles	No puncture or increase of pain when puncturing due to reduced sharpness of microneedle	7	Malfunctioning of 3D printer	5	Use COMSOL to detect incorrect geometry	2	**70**	
Fluid Chamber Reservoir and Microneedle array	Defected Adhesive (silicon glue)	Microneedle device is not properly assembled and cannot deliver therapeutic treatment equally across all 13 nozzles.	7	Damage during device manufacturing or long-term use	4	Developing mechanical test	2	**56**	Routine pressure decay or mass flow testing. Pressure decay: fill part with a volume of air at a specific pressure, isolate part, monitor pressure within part. If there is a decrease in pressure, it indicates leak. Mass flow: part remains connected to an air source to maintain target pressure. If air must be pumped into the device to maintain target pressure this indicates a leak. The flow meter is responsible for the amount of air pumped into the device.

Table 10. User-based Failure Modes and Effects Analysis

Item / Function	Potential Failure Mode(s)	Potential Effect(s) of Failure	Sev	Potential Cause(s)/ Mechanism(s) of Failure	Prob	Current Design Controls	Det	RPN	Recommended Action(s)
13 Microneedle Nozzles	Particulate in microneedles	Contaminants entering patient during administration	9	Improper cleaning techniques	4	Clean using air pump, visual inspection of 13 microneedle array	4	**144**	

13 Microneedle Nozzles	Broken microneedle nozzle	Cannot accurately deliver drug across all 13 microneedles	7	Damage from user	4	Size of nozzle prevents breakage	4	**112**	
13 Microneedle Nozzles	Improper therapeutic administration site	Reduced efficacy of drug due to improper placement of microneedles	4	Unclear instructions, user mishandling	3		2	**70**	Instruct user to administer on arm, in an area where there is no scar tissue
Microencapsulated cell therapeutic	Improper therapeutic delivered	Scheduled drug administration for the patient is disrupted, negatively affected by delivery of improper therapeutic	10	Misreading of label, disorganization of therapeutics	3		7	**36**	Build compatible application to prompt message: check and record label of drug
Microencapsulated cell therapeutic	Contaminated therapeutic	Unsterile therapeutic	9	Improper handling of therapeutic	2	Use sterile gloves when handling therapeutic	7	**36**	
Fluid Chamber Reservoir	Damaged connection to syringe pump	Cannot deliver drug	6	Damage from user or transportation	3		1	**18**	Protective packaging during transport
Flow rate of microcapsules	Improper flow rate used for delivery of therapeutic	Pain is not minimized during drug delivery	4	Improper setting on syringe pump	2	Specified flow rate provided	1	**7**	

Table 11. COMSOL-based Failure Modes and Effects Analysis

Item / Function	Potential Failure Mode(s)	Potential Effect(s) of Failure	Sev	Potential Cause(s)/ Mechanism(s) of Failure	Prob	Current Design Controls	Det	RPN	Recommended Action(s)
13 Microneedle array	Clogged nozzle	Non-uniform administration of therapeutic to patient	5	Particle aggregation, printing defect as a result of shrinkage and inadequate polymerization, uneven microcapsule size distribution	5	Visual inspection of 13 microneedle array	4	**100**	Explore surface coating with charged biocompatible polymer, visual inspection procedure under microscope, conduct Charpy test on microneedle array, reoptimize parameters for the atomization process and reinforce additional microscope inspection step prior to infusion into the device

13 Microneedle array	Suction of microneedle array	Quality of extruded microcapsules is uneven	5	Uneven application of vacuum will cause force to go to a single nozzle this will result in additional shearing of the capsules and cellular damage	5	Visual inspection of 13 microneedle array	4	**100**	Design a vacuum palette to sample evenly from the nozzles for the vacuum force to be distributed evenly.
13 Microneedle array	Dented microneedle	Irreversible damage causing non-uniform administration of therapeutic to patient, improper puncture or incapable of puncturing the epidermis	6	Washing step for removal of non crosslinked polymer was insufficient	4	Visual inspection of 13 microneedle array	3	**72**	Increase wash cycle time post-crosslinking. Prior to use, conduct a visual inspection under microscope and conduct a Charpy test on the microneedle array. Revise pre-submission to 3D printer.
13 Microneedle array	Slightly chipped microneedle	Irreversible damage causing non-uniform administration of therapeutic to patient, improper puncture or incapable of puncturing the epidermis	6	Material is brittle causing a random fracture at that location	4	Visual inspection of 13 microneedle array	3	**72**	Increase wash cycle time post-crosslinking. Prior to use, conduct a visual inspection under microscope and conduct a Charpy test on the microneedle array. Revise pre-submission to 3D printer.
13 Microneedle array	Incorrect geometry of microneedle	Deformation causing non-uniform administration of therapeutic to patient, improper puncture or incapable of puncturing the epidermis	7	CAD defect	3	Visual inspection of 13 microneedle array	3	**63**	Increase wash cycle time post-crosslinking. Prior to use, conduct a visual inspection under microscope and conduct a Charpy test on the microneedle array. Revise pre-submission to 3D printer.

Chapter 5 - Engineering Standards and Constraints

5.1 Manufacturing

The design project meets the engineering standard of being manufacturable due to its production methods. Our design would be fabricated through 3D printing using standard 3D printer materials including photo resin. Due to Covid-19, we were not able to enter the lab and our design project used no materials and therefore did not require manufacturing

5.2 Sustainability

The design project meets the engineering standard of being sustainable because we did not use any materials or biological materials in our project. The device that we are simulating is sustainable when physically manufactured because it proposed a reusable platform. The robust design includes only the syringe to be refillable with matrix between each use making the device more sustainable than a single use hypodermic needle.

5.3 Health and Safety

The design project meets health and safety requirements because no cells were handled and the device was not used to penetrate the skin. For future management of the physical device, cytotoxicity tests need to be performed to ensure the safety of the needle penetrating skin and interacting with the encapsulated cells.

5.4 Social

Additionally, the design project meets social standards because it addresses the problem of minimally invasive drug delivery methods to reduce needle phobia. Microneedles only enter the epidermis layer of the skin and are therefore virtually pain free. People who have a fear of hypodermic needles will be more comfortable and feel safer receiving the care they need through the use of microneedles.

6.5 Economic

Lastly, the design project meets economic standards because we did not order any materials and executed our entire project on COMSOL Multiphysics software. The base COMSOL license cost is $4000, however we had access to a free license through Santa Clara University.

Chapter 6 - Summary and Conclusion

6.1 Summary

The main objective of our project was to model a one phase laminar flow and time-dependent particle trajectory through our custom microneedle device on COMSOL Multiphysics pre-puncture within the therapeutic flow rate for pain minimization. We also aimed to model multiple failure modes of 3D printed artifacts to build a more robust flow profile of our microneedle device. These objectives will lead to an optimized microneedle device that is a minimally invasive system capable of extruding cells transdermally for cell therapy purposes.

The COMSOL laminar flow interface utilizes the Navier Stokes equations which govern the motion of fluids. These equations can be seen as Newton's second law of motion for fluid flow. We ran a single-phase, stationary laminar flow on our device using the following constraints: an inlet velocity of $1.58x10^{-4}$m/s, an inlet pressure of 0 Pa, a dynamic fluid viscosity of 8.90×10^{-4} Pa·s and, a fluid density of 997 kg/m³. The average outlet velocity of the microneedles was $2.82x10^{-3}$m/s or 0.45 mL/min which falls slightly above the therapeutic flow rate range for pain minimization based on the VAS scale. We were able to successfully optimize the flow rate for pain minimization so future handlers of our device will have injection conditions that augment non-invasiveness.

In order to visualize the flow of microencapsulated cells through the device, we ran a time-dependent particle trajectory using the Particle Tracing Module on COMSOL. This module is a general-purpose tool for computing the paths of particles as they travel through a geometry and are subjected to various forces. The particle trajectory constraints we implemented are: a particle diameter of 300μm, a particle density of 1178 kg/m^3, and a particle charge number of 0. After running the particle trajectory simulation on the device, the fastest particles traced are congregated in the needle tip, and the slowest particles are either cemented to the boundary due to the boundary freeze condition in COMSOL or halted at the base of the device. The flow of particles enters the center nozzles at a faster rate than the outer nozzles as a result of the cone-like geometry of the interior of the flow chamber. This geometry was implemented to slow the velocities of the particles through the device to maintain a therapeutic flow rate for pain minimization.

We examined several failure modes that the microneedles could undergo due to a handler error or 3D printing and determined their effect on flow profiles. The first failure mode we investigated was a clogged nozzle. This could occur due to particle aggregation, printing defects as a result of inadequate polymerization, or uneven microcapsule size distribution. When a needle is clogged, the velocity, pressure and impact force of the surrounding nozzles increase. No particles interact with the clogged nozzle because the clogged nozzle does not experience fluid flow. Provisions that may be executed to help reduce the probability of this failure are:

explore the charge of the biocompatible polymer encapsulating the cells, design a visual inspection of the procedure under a microscope, reoptimize parameters for atomization processes and reinforce additional microscope inspections prior to infusion of cells into the device. The next failure mode we investigated is a deformed nozzle. Deformation may be caused by denting due to a short washing process post fabrication, chipping as the material is brittle and easily fractured, or a CAD defect. When the nozzles are deformed in the way that shrinks the nozzle tip, the velocity through the deformed nozzles decreases and the velocity through the non-deformed nozzles increases. The pressure of the deformed nozzles increases and the surrounding nozzle pressures increase very slightly. Particles tended to aggregate in the deformed nozzle but were too large to pass through the needle tip. Provisions that may be executed to help reduce the probability of failure are: increase the wash cycle time after the photoresin has cross-linked, design a visual inspection under the microscope, design a Charpy test for the microneedle array, and revise the CAD submission prior to 3D printing. The last failure mode we simulated is suction. Suction is used to sample microcapsules for quality as a routine test prior to injection for therapeutic purposes. If the vacuum palette is uneven, the force will be applied heavily to a single nozzle. The additional shearing of the capsules causes cellular damage and the damaged cells will not be an accurate sample of extruded microcapsules, rendering the suction test non functional. When suction is applied to a single nozzle of our microneedle system, only that nozzle will experience velocity, pressure, and interact with particles. The velocity and pressure experienced by the failed nozzle is significantly larger than the velocity of the control experiment due to the extreme pressure difference. A provision that may be executed to help reduce the probability of failure is to design a vacuum palette that can evenly sample the nozzles so that the vacuum force does not apply an increased force to a particular nozzle.

6.2 Conclusion

In conclusion, we were successfully able to model a one phase laminar flow and a time-dependent particle trajectory through our custom microneedle device on COMSOL Multiphysics pre-puncture within the therapeutic flow rate for pain minimization. We also successfully modeled multiple failure modes of 3D printed artifacts to build a more robust flow profile of our microneedle device. Our device is a non-invasive and targeted method for cell delivery into the epidermis layer of the skin for therapeutic usage.

6.3 Future Work

In upcoming experimental studies, deviations from expected flow patterns will enable the measurement of shear experienced by microencapsulated cells, and their subsequent viability. Building new automated soft sensors enabled by the simulated library of flow defects in conjunction with cell viability studies will generate training sets for validation studies through machine learning.

Fujifilm Prescale pressure sensitive paper in the Ulta Extreme Low pressure range (0.87-7.3 PSI) was sourced from Sensor Products Inc. The paper reacts to pressure by breaking microcapsules when force is applied creating an image indicating where the greatest color change is relative to the highest impact force. This result can be analyzed by Sensor Product Inc. to provide quantitative results in PSI. In future works pressure sensitive paper would serve to experimentally validate the exit pressure predicted by the laminar flow model.

Chapter 7 - References

[1] Al-Dulimi, Z., Wallis, M., Tan, D. K., Maniruzzaman, M., & Nokhodchi, A. (2020, November 16). 3D printing technology as innovative solutions for biomedical applications. *Drug Discovery Today*. https://www.sciencedirect.com/science/article/pii/S1359644620304785?casa_token=-9QsnWhvkWIAAAAA%3Ab52I5YxUYJ-IjGmP8CYvGs9quIlxophiTPWRD1evTRRGOueTRBTyiKJ_KdukmvZKbNJWexbFqg.

[2] Cheung, K. & Das, D. (2016) Microneedles for drug delivery: trends and progress, Drug Delivery. *Taylor & Francis Group*.

[3] Cowen, R., Stasiowska, M. K., Laycock, H., & Bantel, C. (2015). Assessing pain objectively: the use of physiological markers. *Anaesthesia*, 70(7), 828-847.

[4] Economidou, S. N., & Douroumis, D. (2021, March 26). 3D printing as a transformative tool for microneedle systems: Recent advances, manufacturing considerations and market potential. *Advanced Drug Delivery Reviews*. https://www.sciencedirect.com/science/article/pii/S0169409X21000739?casa_token=L1NrJQZHAgEAAAAA%3AMYGbQtAEoon_Czjl6yLwv1kl7cRYTxyFa5AQw0dRCeEt9GAyH8wSB4KSKv9vNhfCblVKZGSfgQ.

[5] Farias, C., Lyman, R., Hemingway, C., Chau, H., Mahacek, A., Bouzos, E., & Mobed-Miremadi, M. (2018). Three-Dimensional (3D) Printed Microneedles for Microencapsulated Cell Extrusion. *Bioengineering*.

[6] Formlabs, Inc. The Ultimate Guide to Stereolithography (SLA) 3D printing. 2017. *Formlabs.com.*

[7] Gill HS, Denson DD, Burris BA, Prausnitz MR. Effect of microneedle design on pain in human subjects. *The Clinical journal of pain*. 2008;24(7):585-594. doi:10.1097/AJP.0b013e31816778f9.

[8] Gualeni, B., Coulman, S.A., Shah, D., Eng, P.F., Ashraf, H., Vescovo, P., Blayney, G.J., Piveteau, L.-D., Guy, O.J. and Birchall, J.C. (), Minimally-invasive and targeted therapeutic cell delivery to the skin using microneedle devices. *Br J Dermatol*. Accepted Author Manuscript. doi:10.1111/bjd.15923

[9] Gudipaty, S., & Rosenblatt, J. (2017). Epithelial cell extrusion: Pathways and pathologies. *Elsevier*.

[10] Gupta J; Park SS; Bondy B; Felner EI; Prausnitz MR;. (2011, June 17). Infusion pressure and pain during microneedle injection into skin of human subjects.

[11] Ita K. Transdermal Delivery of Drugs with Microneedles—Potential and Challenges. Olatunji O, ed. *Pharmaceutics*. 2015;7(3):90-105. doi:10.3390/pharmaceutics7030090.

[12] Krieger, K. J., Bertollo, N., Dangol, M., Sheridan, J. T., Lowery, M. M., & O'Cearbhaill, E. D. (2019, September 9). Simple and customizable method for fabrication of high-aspect ratio microneedle molds using low-cost 3D printing. *Nature News*. https://www.nature.com/articles/s41378-019-0088-8.

[13] Malcolm, X., & Malcolm, X. (2021, January 29). Trypanophobia- A Fear of Needles. *Health Beat*. https://jamaicahospital.org/newsletter/trypanophobia-a-fear-of-needles/.

[14] Mansor, N. H. A., Markom, M. A., Tan, E. S. M. M., & Adom, A. H. (2019, November 1). Design and Fabrication of Biodegradable Microneedle Using 3D Rapid Prototyping Printer. *Journal of Physics: Conference Series*. https://iopscience.iop.org/article/10.1088/1742-6596/1372/1/012053/meta.

[15] McLenon J, Rogers MAM. The fear of needles: A systematic review and meta-analysis. *J Adv Nurs*. 2019 Jan;75(1):30-42. doi: 10.1111/jan.13818. Epub 2018 Sep 11. PMID: 30109720.

[16] McMaster, M. C., & HPLC, A. (1998). A Practical User's Guide(p. 4). *Wiley-Vch*.

[17] Meng, F., Hasan, A., Babadaei, M. M. N., Kani, P. H., Talaei, A. J., Sharifi, M., Cai, T., Falahati, M., & Cai, Y. (2020, August 1). Polymeric-based microneedle arrays as potential platforms in the development of drugs delivery systems. *Journal of Advanced Research*. https://www.sciencedirect.com/science/article/pii/S2090123220301764?via%3Dihub.

[18] *Microencapsulation Technology.* (2021). Watson Inc. https://www.watson-inc.com/our-capabilities/microencapsulation/.

[19] Mohammed, A., Elshaer, A., Sareh, P., Elsayed, M., & Hassanin, H. (2020, March 20). Additive Manufacturing Technologies for Drug Delivery Applications. *International Journal of Pharmaceutics*. https://www.sciencedirect.com/science/article/pii/S0378517320302295?casa_token=zou65thr-bgAAAAA%3A8oy80U73E-Gdc1lMLQHLBwHNgpPmBwjbhVYzf0l_esrqxO4Mt32tVVfJWQi1mVeesK93CzFXCA.

[20] Nur Hazwani Azyan, M., Marni Azira, M., Erdy Sulino, M. M. T., & Abdul Hamid, A. (1970, January 1). Design and Fabrication of Biodegradable Microneedle Using 3D Rapid

Prototyping Printer. *DSpace Home*.
http://dspace.unimap.edu.my/xmlui/handle/123456789/69031.

[21] Prausnitz, Mark R. (2004). Microneedles for Transdermal Drug Delivery. 56(5): 581-587. doi.org/10.1016/j.addr.2003.10.023.

[22] Tabatabaian, M. (2015). CFD Module: The Ultimate Guide to Stereolithography (SLA) 3D Printing. Formlabs. *Stylus Publishing, LLC*.
https://formlabs.com/blog/ultimate-guide-to-stereolithography-sla-3d-printing/.

[23] Tucak, A., Sirbubalo, M., Hindija, L., Rahić, O., Hadžiabdić, J., Muhamedagić, K., Čekić, A., & Vranić, E. (2020, October 27). *Microneedles: Characteristics, Materials, Production Methods and Commercial Development. MDPI*. https://www.mdpi.com/2072-666X/11/11/961.

[24] Wallis, M., Al-Dulimi, Z., Tan, D., Maniruzzaman, M., & Nokhodchi, A. (2020). 3D printing for enhanced drug delivery: current state-of-the-art and challenges. *Taylor & Francis.* https://www.tandfonline.com/doi/full/10.1080/03639045.2020.1801714.

[25] Xenikakis, I., Tsongas, K., Tzimtzimis, E. K., Zacharis, C. K., Theodoroula, N., Kalogianni, E. P., Demiri, E., Vizirianakis, I. S., Tzetzis, D., & Fatouros, D. G. (February 2, 2021). Fabrication of hollow microneedles using liquid crystal display (LCD) vat polymerization 3D printing technology for transdermal macromolecular delivery. *International Journal of Pharmaceutics*.
https://www.sciencedirect.com/science/article/pii/S0378517321001071?casa_token=MuqvRvyTV4YAAAAA%3An0gbBNSdtYO_YjIGKJWKCpKxQMdr070QwVQq7W0FuzNiFuxK4kYi0SMrfjC6eLWMjxnEmd7WiA.

[26] Yao, W., Li, D., Zhao, Y., Zhan, Z., Jin, G., Liang, H., & Yang, R. (December 23, 2019). 3D Printed Multi-Functional Hydrogel Microneedles Based on High-Precision Digital Light Processing. *MDPI.* https://www.mdpi.com/2072-666X/11/1/17.

[27] Yeung, C., Chen, S., King, B., Lin, H., King, K., Akhtar, F., Diaz, G., Wang, B., Zhu, J., Sun, W., Khademhosseini, A., & Emaminejad, S. (December 11, 2019). A 3D-printed microfluidic-enabled hollow microneedle architecture for transdermal drug delivery. *AIP Publishing*. https://aip.scitation.org/doi/full/10.1063/1.5127778.

[28] Marchi, Antonio & Vellucci, Renato & Mameli, Sergio & Piredda, Anna & Finco, Gabriele. (2009). Pain Biomarkers. *Clinical drug investigation*. 29. Supplement 1. 41-46. 10.2165/0044011-200929001-00006.

[29] Relland, L. M., Gehred, A., & Maitre, N. L. (October 10, 2018). Behavioral and Physiological Signs for Pain Assessment in Preterm and Term Neonates During a

Nociception-Specific Response: A Systematic Review.
https://www.sciencedirect.com/science/article/pii/S0887899418306672c

Chapter 8 - Appendix

8.1 Other Deformed Nozzle Simulations

8.1.1 Increased Tip Diameter

To simulate an increased tip diameter, which may have been caused by a breakage, we increased the diameter of the center nozzle from 400 micrometers to 600 micrometers. Figure X demonstrates the results from the laminar flow and particle trajectory.

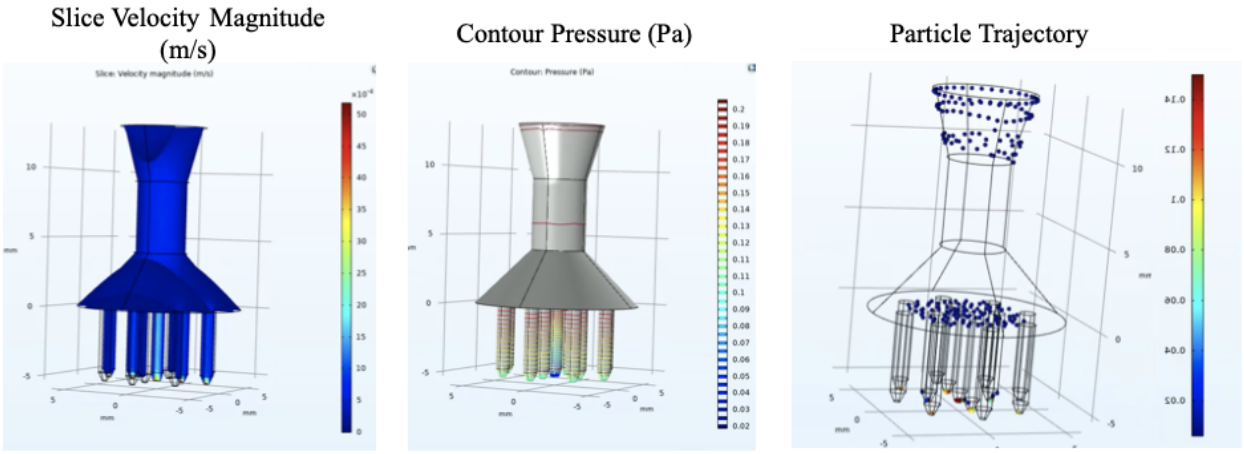

Figure 21. Velocity, pressure, and particle trajectory plots demonstrating suction on the center needle with an increased diameter of 600 microns.

The outlet velocity of the center nozzle that has a tip diameter of 600 micrometers is 3.7×10^{-3} m/s while the remaining nozzles had a velocity of 5.1×10^{-3} m/s. If the needle tip has a larger diameter, then it will experience a slower velocity extruding through the nozzle. The pressure of the center nozzle was about 0.04 Pa while the remaining nozzles had an increased pressure of 0.14 Pa. More particles were able to travel to the tip of the center nozzle due to its larger diameter. Particle trajectory did not show any significant discrepancies with a larger tip diameter.

The impact force graphs show that the center nozzle had a higher impact force than the remaining nozzles due to its larger surface area. The impact force of the center nozzle is 2.8×10^{-6}N while the unchanged needles have an impact force of 1.0×10^{-6} N.

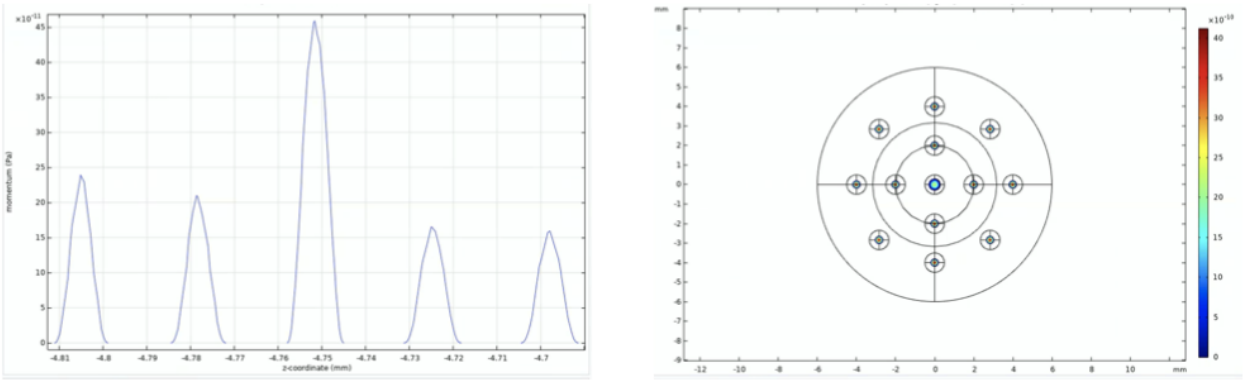

Figure 22. (a) One dimensional graph of impact force plot of 5 needles with center nozzle at a 600 micron diameter. (b) Plane plot of impact force of all 15 needles with center nozzle at a 600 micron diameter.

8.1.2 Slated Tip

To simulate a slanted nozzle tip, we modeled the geometry in 2D to create a more accurate model for our failure mode. We simulated a slanted tip by making the right corner of the tip 200 micrometers above the left corner of the tip in 2D. Based on this geometry, the new diameter of the tip is 447.2 micrometers.

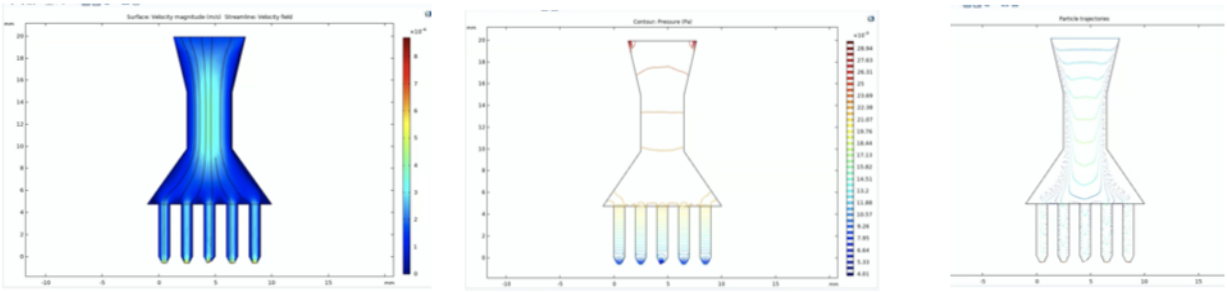

Figure 23. 2D velocity, pressure, and particle trajectory plots demonstrating a slanted center nozzle.

The outlet velocity of the slanted needle is 3.7×10^{-4} m/s while the remaining nozzles have an outlet velocity of 3.5×10^{-4} m/s. The particle trajectory plot experienced no significant discrepancies.